AD-A038 590 DAVID W TAYLOR NAVAL SHIP RESEARCH AND DEVELOPMENT CE--ETC F/G 13/7
HYDRODYNAMIC PERFORMANCE OF THE MODEL OF A VARIABLE AREA WATERJ--ETC(U)
FEB 77 A D SOBOLEWSKI

UNCLASSIFIED SPD-735-01 NL

1 OF 2
ADA038590

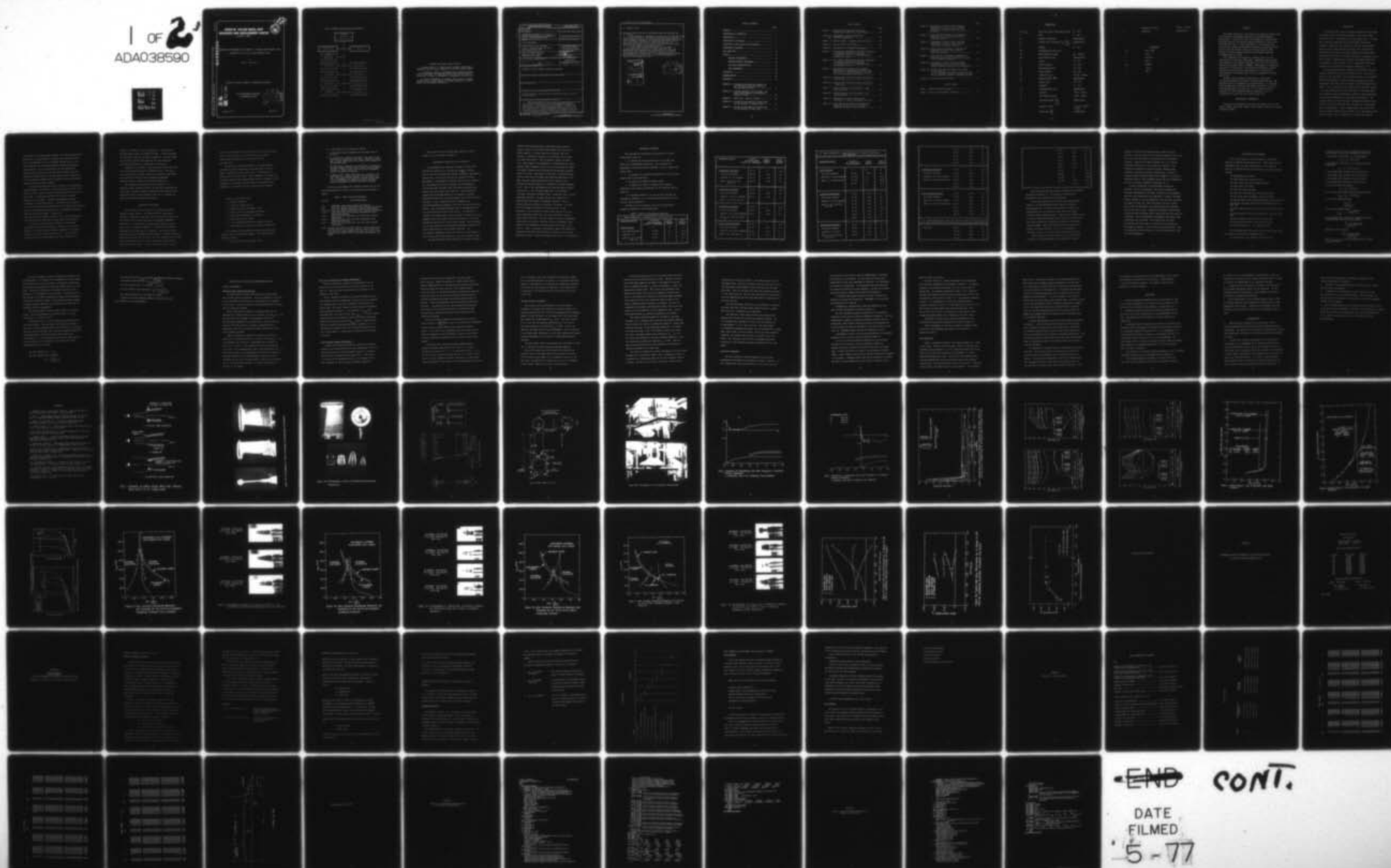

~~END~~ CONT.

DATE
FILMED
5-77

1 OF 2

ADA038590

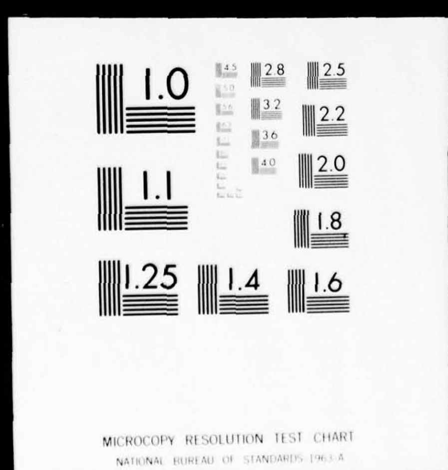

SPD-735-01

HYDRODYNAMIC PERFORMANCE OF THE MODEL OF A VARIABLE AREA WATERJET INLET DESIGNED FOR A 200 TON, 100 KNOT HYDROFOIL SHIP

(12)

DAVID W. TAYLOR NAVAL SHIP RESEARCH AND DEVELOPMENT CENTER

Bethesda, Md. 20084

HYDRODYNAMIC PERFORMANCE OF THE MODEL OF A VARIABLE AREA WATERJET INLET DESIGNED FOR A 200 TON, 100 KNOT HYDROFOIL SHIP

by

Alan D. Sobolewski

APPROVED FOR PUBLIC RELEASE: DISTRIBUTION UNLIMITED

SHIP PERFORMANCE DEPARTMENT

DEPARTMENTAL REPORT

February 1977

SPD-735-01

MAJOR DTNSRDC ORGANIZATIONAL COMPONENTS

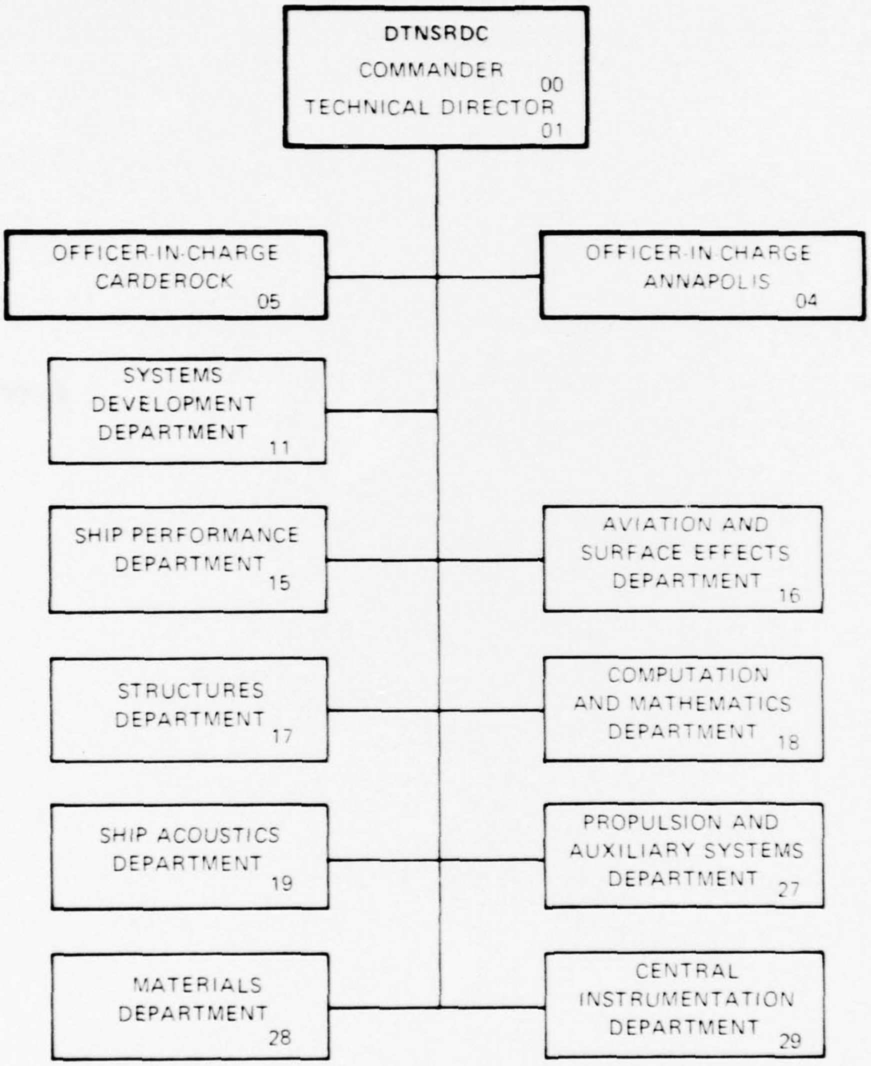

GPO 905-678

NDW-DTNSRDC 3960/43b (Rev. 11-75)
GPO 928-108

DTNSRDC ISSUES THREE TYPES OF REPORTS

(1) DTNSRDC REPORTS, A FORMAL SERIES PUBLISHING INFORMATION OF PERMANENT TECHNICAL VALUE, DESIGNATED BY A SERIAL REPORT NUMBER.

(2) DEPARTMENTAL REPORTS, A SEMIFORMAL SERIES, RECORDING INFORMATION OF A PRELIMINARY OR TEMPORARY NATURE, OR OF LIMITED INTEREST OR SIGNIFICANCE, CARRYING A DEPARTMENTAL ALPHANUMERIC IDENTIFICATION.

(3) TECHNICAL MEMORANDA, AN INFORMAL SERIES, USUALLY INTERNAL WORKING PAPERS OR DIRECT REPORTS TO SPONSORS, NUMBERED AS TM SERIES REPORTS; NOT FOR GENERAL DISTRIBUTION.

SECURITY CLASSIFICATION OF THIS PAGE (When Data Entered)

REPORT DOCUMENTATION PAGE		READ INSTRUCTIONS BEFORE COMPLETING FORM
1. REPORT NUMBER 14 SPD-735-Ø1	2. GOVT ACCESSION NO.	3. RECIPIENT'S CATALOG NUMBER
4. TITLE (and Subtitle) 6 HYDRODYNAMIC PERFORMANCE OF THE MODEL OF A VARIABLE AREA WATERJET INLET DESIGNED FOR A 200 TON, 100 KNOT HYDROFOIL SHIP,		5. TYPE OF REPORT & PERIOD COVERED 6. PERFORMING ORG. REPORT NUMBER
7. AUTHOR(s) 10 Alan D. Sobolewski		8. CONTRACT OR GRANT NUMBER(s)
9. PERFORMING ORGANIZATION NAME AND ADDRESS David W. Taylor Naval Ship R&D Center Bethesda, Maryland 20084 3 Ship Perf. Dept		10. PROGRAM ELEMENT, PROJECT, TASK AREA & WORK UNIT NUMBERS Task Areas S 324613 and SF 43270201, Elements 62543N and 63508N
11. CONTROLLING OFFICE NAME AND ADDRESS Naval Sea Systems Command Washington, D.C. 20350		12. REPORT DATE 11 Feb 1977 13. NUMBER OF PAGES 12 91p.
14. MONITORING AGENCY NAME & ADDRESS (if different from Controlling Office) 16 S3246, F43270 17 S324613, SF43270201		15. SECURITY CLASS. (of this report) UNCLASSIFIED 15a. DECLASSIFICATION/DOWNGRADING SCHEDULE

16. DISTRIBUTION STATEMENT (of this Report)

APPROVED FOR PUBLIC RELEASE: DISTRIBUTION UNLIMITED

17. DISTRIBUTION STATEMENT (of the abstract entered in Block 20, if different from Report)

18. SUPPLEMENTARY NOTES

19. KEY WORDS (Continue on reverse side if necessary and identify by block number)

100 Knot Hydrofoil, Pod-Strut Inlets, Variable-Area Inlets, Cavitation, Pressure Recovery

20. ABSTRACT (Continue on reverse side if necessary and identify by block number)

The primary objective of this study was to assess the state-of-the-art in waterjet inlet design capability for high-speed hydrofoil applications. A contract was let for the design of a variable-area, strut-pod inlet for the waterjet propulsion system of a 200 ton, 100 knots hydrofoil ship. A basic requirement of the design was that the inlet must provide cavitation-free operation for prescribed flow-rates at both the 100 knots cruise and 35 knots take-off speed. The most → next page

DD FORM 1473 1 JAN 73 EDITION OF 1 NOV 65 IS OBSOLETE
S/N 0102-014-6601

UNCLASSIFIED
SECURITY CLASSIFICATION OF THIS PAGE (When Data Entered)

389694

20. ABSTRACT (cont.)

up-to-date design procedures and performance prediction techniques were to be used.

After completion of the design, a contract was let for the construction of a one-fifth scale model. Experiments with the model were conducted in the waterjet loop facility of the 36-inch Variable Pressure Water Tunnel (VPWT) at DTNSRDC. Measurements or observations were made of the drag force, inlet pressure distribution, internal pressure loss, and cavitation characteristics. The results of this evaluation are reported here as they are compared with design predictions.

At water tunnel conditions simulating the cruise speed, the model demonstrated the ability to operate cavitation free. The measured data are in agreement with the predictions. At off-design model configurations (retracted centerbody), the data do not show a good agreement with the predictions. At the simulated take-off condition, the model exhibited internal cavitation at an IVR corresponding to about 95% of the required flow rate.

TABLE OF CONTENTS

LIST OF FIGURES

LIST OF TABLES

NOMENCLATURE

A, A_i, A_{i_c}	area, inlet area, inlet area (cruise)	ft^2 (m^2)
C	chord	ft (m)
C_P	pressure coefficient	dimensionless
C_{P_L}	pressure loss coefficient, $C_{P_L} = \frac{\Delta H}{\frac{1}{2}\rho V_\infty^2}$	dimensionless
D	diameter	ft (m)
DSI	Developmental Sciences Inc.	
ΔH	head (pressure) losses	psi (pascal)
IVR	inlet velocity ratio	dimensionless
L	length	ft (m)
P	static pressure	psi (pa)
P_L	head (pressure) loss	psi (pa)
P_T	total pressure	psi (pa)
Q	volume flow rate	ft^3/sec (m^3/sec)
Re	Reynolds number $\frac{V \cdot D}{\gamma}$	dimensionless
S	surface area	ft^2 (m^2)
t	thickness	ft (m)
t/c	thickness/chord ratio	dimensionless
V	velocity	ft/sec (m/sec)
V_∞	free stream velocity	ft/sec (m/sec)
σ	cavitation number $\frac{P-P_V}{\frac{1}{2}\rho V_\infty^2}$	dimensionless
ρ	density of water	$\frac{Lb_f \, sec^2}{ft^4}$ (kg/m^3)
λ	scale ratio $(\frac{L_P}{L_m})$	dimensionless

γ	kinematic viscosity	ft^2/sec (m^2/sec)
η	efficiency	dimensionless

Subscripts

∞,0	free stream
i	inlet
P	prototype
m	model
min	minimum
c	cruise
v	vapor

ABSTRACT

The primary objective of this study was to assess the state-of-the-art in waterjet inlet design capability for high-speed hydrofoil applications. A contract was let for the design of a variable-area, strut-pod inlet for the waterjet propulsion system of a 200 ton, 100 knots hydrofoil ship. A basic requirement of the design was that the inlet must provide cavitation-free operation for prescribed flow-rates at both the 100 knots cruise and 35 knots take-off speed. The most up-to-date design procedures and performance prediction techniques were to be used.

After completion of the design, a contract was let for the construction of a one-fifth scale model. Experiments with the model were conducted in the waterjet loop facility of the 36-inch Variable Pressure Water Tunnel (VPWT) at DTNSRDC. Measurements or observations were made of the drag force, inlet pressure distribution, internal pressure loss, and cavitation characteristics. The results of this evaluation are reported here as they are compared with design predictions.

At water tunnel conditions simulating the cruise speed, the model demonstrated the ability to operate cavitation free. The measured data are in agreement with the predictions. At off-design model configurations (retracted centerbody), the data do not show a good agreement with the predictions. At the simulated take-off condition, the model exhibited internal cavitation at an IVR corresponding to about 95% of the required flow rate.

ADMINISTRATIVE INFORMATION

The project was sponsored by the Naval Sea Systems Command, Code (0332) (03411), Task Areas S 324613 and SF 43270201, Task 17867, Elements 62543N and 63508N.

INTRODUCTION

The Navy has been involved in several programs to develop high performance craft with waterjet propulsion. The craft concepts include the S.E.S., the hydrofoil, and the planing craft. In recent years, numerous feasibility and advanced design studies were conducted. Along with such studies, the Navy has had operational experience with several waterjet propelled craft including the hydrofoils: PGH-2 Tucumcari, and PHM-1 Pegasus; the surface effect ships; XR-1 and SES 100-A, and some planing boats. In addition to the Navy's efforts, numerous state-of-the-art and design reports are now available in the literature. Some of those which offer good background on the subject are included as References 1 to 9.

The work, reported herein, addresses the feasibility of using waterjet propulsion for very fast hydrofoil craft. The critical problem is the availability of the required thrust at both take-off speed and cruise speed. In order to match the hydrofoil's thrust requirements, high flow rates are needed at both hump speed and top speeds. Thus, a fixed-area inlet operates with a low IVR, $(V_{in}/V_{\infty}) < 1$, at top speed and with a high IVR, IVR>>1, at the hump speed. Such operation requires considerable variation of inflow angle with the resultant susceptibility to cavitation (See Figure 1). The principal feature of the inlet which influences the range of inlet velocity ratios over which the inlet can operate is its thickness near the leading edge. A thick leading edge of the inlet can be used to provide cavitation free operation over a wide range of inlet velocity ratios. But, a large part of the total inlet drag is

proportional to the leading edge thickness. The body characteristics, which lead to a minimal amount of external drag, require the inlet and its leading edge to be of the smallest workable size. So, the inlet design must be a compromise between its drag and cavitation characteristics. For best performance, the inlet design must achieve a noncavitating inlet lip shape for the design value and required off-design values of the inlet velocity ratio, dictated by the craft operation schedule, while retaining a shape with favorable external drag at the cruise condition.

This problem becomes more acute as the ratio of top-speed/hump-speed increases. For instance, a very fast hydrofoil may have a top speed of 100 knots while its take-off speed would still be in the 30 knots range. A fixed-area inlet would not be able to perform adequately at both speeds. Variable-area mechanism are being investigated for these applications. The object of this scheme is to vary the inlet flow area inversely with craft speed, holding the inlet velocity ratio relatively constant, so as to accomodate the required mass flow rate at both speeds. Holding the inlet velocity ratio constant allows for a very thin leading edge of the inlet nose which should have favorable drag characteristics.

In order to assess the state-of-the-art of inlet design technology for high speed hydrofoils, a contract was let for the design of a variable-area inlet-diffuser component of the waterjet system of a 200 ton, 100 knot hydrofoil craft. The preliminary powering and flow rate requirements which were provided to the

contractor by DTNSRDC are given in Appendix A. The design was performed under contract No. N00600-73-C-0964. The work statement and deliverable items are included in Appendix B. The final report on the subject contract which describes the inlet design and performance predictions is included here as Reference 10.

Subsequent to the design, a one-fifth scale model of the inlet was constructed under contract No. N00600-75-C-0425. This scale ratio was selected to provide a model size suitable for experiments with the waterjet flow-loop and six-component dynamometer (Reference 11)at the DTNSRDC 36-inch VPWT (Reference 12).

The experiments described herein were conducted to (1) evaluate the drag, pressure recovery, and cavitation characteristics of the model at scaled conditions, representing the speed flow rate operational envelope of the prototype inlet, and (2) validate the design and performance prediction techniques.

DESCRIPTION OF THE MODEL

The one-fifth scale (λ=5) model of the strut-pod inlet was constructed under contract. The selection of this scale ratio provided a conveniently sized model for the 36-inch water tunnel and the waterjet flow loop with associated six-component dynamometer (Reference 11). Pod-strut data including model dimension, table of offset, etc. are included in Appendix C. Figures 2A and B present photographs of the model and it's components. The distance from the pod centerline to the dynamometer mating flange of the model (model strut height) was selected to be 32.4 inch. This strut height places the center of the model pod near the test section centerline, which minimizes tunnel interference effects. As such, the models internal flow path

in the strut represents only the lower 75% of the 18 foot prototype strut. Also, that part of the model strut with the proper external shape represents only the lower half of the prototype strut.

The model was constructed primarily of anodized aluminum including the movable centerbody, the turning vanes, the outer shell, a removable lip with pressure taps, a faired boat tail section, and a solid nose piece. Other components of the model are typically stainless steel including the flange for attachment to the dynamometer, the pressure taps and tubing, and centerbody drive components. An alternate lip made of lexan was also provided.

Features of the model include:

1. A movable centerbody
2. A vaned turn within the pod
3. A parabolic strut, blunt based, t/c=12%
4. A faired, boat tail afterbody for the pod
5. A blunt base configuration for the pod
6. A solid nose piece (no inlet)
7. A lip, instrumented with static pressure tap holes
8. A transparant lip, (lexan) for cavitation observation

The centerbody was controlled from outside the water tunnel through a series of mechanical linkages. The centerbody drive components include:

1. A high pitch ball-screw within the pod

2. A right-angle drive at the base of the pod

3. A long vertical shaft extending from the angle drive of the strut

4. An offset drive; connecting the shaft at the strut to the sealed driver through the tunnel shell, consisting of shafting, universal angle drives, and sliding torque linkage (no thrust-torque only).

5. The main driver, located on the tunnel shell, consisting of the shaft through the tunnel shell (sealed from the tunnel) coupled to a stepper motor, with clutch, and a handwheel override for manual positioning.

6. A magnetic disc, pickup, and counter were attached to the main driver for a digital display of the centerbody position. This magnetic pick-up/counter system, used to monitor the centerbody, was capable of accurate centerbody position measurement to within 0.005 inch (0.135 mm).

The model was instrumented with numerous pressure taps for the various measurements as listed in the following table and shown in Figure 3.

TABLE 1 - Model Pressure Measurements

Tap Nos.	Location/Measurement
1-4	Centerbody, axial static pressure distribution
5-8	Inlet lip, internal peripheral static pressure distribution
9-13	Inlet lip, external axial static pressure distribution
11, 14-16	Inlet lip, external peripheral static pressure distribution
17-20	Lower strut wall, strut internal longtitudinal static pressure distribution
21-25	Lower strut flow centerline, strut flow total pressure distribution
26-28	Upper strut wall, strut internal longitudinal static pressure distribution
29-35	Upper strut flow centerline, strut flow total pressure distribution

Note: Pressure taps #29-35 each were capable of being indexed across the width of the strut internal flow area and as such could have provided a rather complete flow map, but, because of the extensive test agenda, only the centerline measurements were taken.

Other pod-strut data including model dimension, table of offsets, etc. are included in Appendix C.

DESCRIPTION OF THE FACILITY AND APPARATUS

The experiments were conducted at DTNSRDC's 36-inch VPWT (described in Reference 12) utilizing the waterjet flow-loop facility with the associated six-component dynamometer (described in Reference 11). The flow-loop facility was modified for these experiments. The dynamometer's mounting base had to be enlarged to fit, the piping circuit was re-arranged, and the dynamometer inverted such that the model inlet flow passes down through the bottom of the test section (See Figure 4A). This modification insures that the minimum pressure of the manometer (pressure measurement) system and of the model-piping flow loop is located at the model. In the original flow-loop arrangement, the mounting-base/piping and manometer tubes were located atop the test section. Thus, the minimum pressure point of the manometers and flow circuit was also atop the test section. At conditions of extremely low pressure there could be problems of water vapor in the manometer lines and possible insufficient pressure to force water through the flow circuit or flow circuit choking. The now modified flow circuit allows for better pressure measurement capability and better identification of inlet choking conditions. The six-component dynamometer (Figure 4B) was found to work equally as well in this layout (upside down) as it was in the original layout.

The data-acquisition system consisted of eighteen transducer

elements with associated signal conditioning units, analog to digital converter, an Interdata model computer with 36K bytes of memory capacity, a Tri-data cartrifile continuous loop tape recorder, a strip-chart recorder, an oscilloscope, and a Printec high speed line printer. The 18 transducer elements include: 6 force "block" gages in the dynamometer, a "Ronningen-Petter" static pressure sensor installed in the flow loop just outside the tunnel, an "Annubar" flow-meter with differential pressure gage installed ahead of the pump, a mag-pickup for pump rpm, a "Bailey"flow-meter (orifice type) with the pressure gage installed downstream of the pump, the water tunnel pressure and velocity sensors, and 6 differential pressure gages with a "Scanivalve" pressure switching device. Most of the instrumentation has been described previously (Reference 11). The 6 pressure gages were of the variable reluctance, differential pressure types, ("Validyne") with ±20 psid diaphragms installed. All gages had one port connnected to a manifold which was exposed to atmospheric pressure. Thus, a constant reference pressure is available to each gage. The other side of each gage is exposed to the collector part of the Scanivalve. The scanivalve can collect data from any one of the twelve measurement ports which are in turn connected to pressure sensors within the model. The total number of pressure measurements taken during a run was 42. With the use of the scanivalve, these pressures were sequentially recorded through the 6 gages, 6 at a time for 7 times. Along with the scanivalve, gages, and plumbing an appropriate fresh water bleed system was installed in the pressure measurement system to insure the plumbing would be free of entrapped air.

EXPERIMENTAL PROCEDURE

This experimental investigation was undertaken to achieve certain goals; these are:

1. To quantify the drag characteristics of the model and relate them to performance predictions; and to compare the performance of the pod with inlet operating to that of a simple pod without inlet.

2. To establish the cavitation characteristics of the pod and compare these to the predictions.

3. To quantify the internal pressure losses.

4. To quantify the effect of changing inlet operating conditions on the pressure distributions of the centerbody and the inlet lip.

5. To determine whether or not the pod inlet provides the performance required of it in a waterjet propulsion system for the 200 ton, 100 knot Hydrofoil.

The matrix of test conditions used for this experimental program is presented in the following table.

TABLE 2 - Matrix of Experimental Conditions

I. Model configuration: instrumented lip, faired boat tail			
Centerbody Position	Simulated Full Scale Speed (Knots)(ft. submergence)	Tunnel Pressure (PSIA)	Tunnel Velocity (ft/sec)
Fully Retracted	0	15	0
full scale reference	20 (18)	10	22.05
position = 0.0	35 (18)	10	38.59
model = -1.3 in. from inlet lip	35 (4)	4	27.6
	0	4	0

Centerbody Position	Simulated Full Scale Speed (Knots) (ft. submergence)	Tunnel Pressure (PSIA)	Tunnel Velocity (ft/sec)
Intermediate Deployment	35 (4)	4	27.6
full scale reference	60 (4)	2.99	40
position = 15 in. extended	60 (4)	1.89	30
model = +1.455 in. from inlet lip	80 (4)	1.89	40
Intermediate Deployment	35 (4)	4	27.6
full scale reference	60 (4)	1.89	30
position = 24.44 in. extended	80 (4)	1.89	40
model = +3.34 inch from lip			
Intermediate Deployment	35 (4)	4	27.6
full scale reference	50 (4)	1.89	30
position = 30.73 inch extended	80 (4)	1.89	40
model = +4.6 inch from inlet lip			
Fully Extended Deployment	35 (4)	4	27.0
full scale reference	50 (4)	1.89	30
position = 34.73 inch extended	80 (4)	1.89	40
model = +5.4 inch from lip	100 (4)	1.39	40

II. Model Configuration: Lexan Inlet Lip for cavitation observation, blunt based pod			
Centerbody Position	Simulated Full Scale Speed	Tunnel Pressure	Tunnel Velocity
Fully Retracted	0	15	0
full scale reference	10 (18)	8.35	10
position = 0.0 inch extended	20 (18)	10	22.05
model = -1.3 inch from lip	35 (18)	10	38.59
	35 (4)	4	27.6
	0	4	0
Intermediate Deployment	40 (4)	2.70	25
full scale reference	40 (4)	3.68	30
position = 15 inch extended	40 (4)	4.84	35
model = +1.455 inch from inlet lip	40 (4)	2.73	25
	35 (4)	4.00	27.6
	40 (4)	1.90	20
	50 (4)	1.90	25
	60 (4)	1.90	30
Intermediate Deployment	40 (4)	2.70	25
full scale reference	40 (4)	3.86	30
position = 24.44 inch	40 (4)	4.84	35
model = +3.34 inch from inlet lip	35 (4)	4.00	27.6

	40 (4)	1.90	20
	50 (4)	1.90	25
	60 (4)	1.90	30
	70 (4)	1.90	35
	80 (4)	1.90	40
<u>Intermediate Deployment</u>	35 (4)	4.0	27.6
full scale reference	40 (4)	1.90	20
position = 20.73 inch extended	50 (4)	1.90	25
model =+4.6 inch from inlet lip	60 (4)	1.90	30
	70 (4)	1.90	35
	80 (4)	1.90	40
<u>Fully Extended Deployment</u>	40 (4)	1.90	20
full scale reference	50 (4)	1.90	25
position = 34.73 inch extended	60 (4)	1.90	30
model = +5.4 inch from inlet lip	70 (4)	1.90	35
	80 (4)	1.90	40
	90 (4)	1.90	45
	100 (4)	1.90	40
III. Model Configuration: Solid nose piece (no inlet) with blunt base pod			
(no-inlet)	100 (4)	1.39	40
	80 (4)	1.89	40
	90 (4)	1.89	45
	70 (4)	1.89	35

60 (4)	1.89	30
50 (4)	1.89	25
40 (4)	1.89	20
40 (4)	2.70	25
40 (4)	3.68	30
40 (4)	4.84	35
35 (4)	4	27.6
35 (18)	10	38.59
20 (18)	10	22.05
10 (18)	8.35	10.0
0	14.54	0

Water tunnel-start-up and testing procedures were followed as described in Reference 11. The procedure to establish the experimental test condition is described below.

Free stream speed and inlet flow rate were simultaneously brought up to the predetermined tunnel speed and a typical non-cavitating IVR. The free stream pressure was reduced to a predetermined value to establish a water tunnel free stream cavitation number (simulated speed). Inlet flow was reduced to near or slightly cavitating condition on the exterior of the inlet lip. Free stream pressure was re-adjusted to attain the free stream cavitation number. Inlet flow was again varied to establsh (1) external cavitation inception, (2) 1/2 to 1 inch external cavitation, and (3) 1 to 2 inch external cavitation at the lip.

After taking data at these conditions, the inlet flow was increased in 100 gpm increments with re-adjustment of tunnel

pressure to hold the free stream cavitation number for each condition. Data was taken at each successive increase in flow rate. Then, inlet flow was adjusted to establish internal cavitation inception. Inlet flow was again increased for 2 or 3 internal cavitating conditions up to the choked flow condition. This procedure was repeated for several different simulated speed conditions to establish cavitation boundaries as a function of cavitation number (simulated speed) and IVR ($\frac{V_{in}}{V_\infty}$) for a particular centerbody position. The centerbody position was then changed and a new set of cavitation boundaries established for it.

Several calibrations of the measurement systems were performed. Before the experiment, the force block-gages were calibrated individually on the bench, installed in the dynamometer, which was then calibrated for six components of loading, including multiple loading in the test-calibration stand, and then calibrated once again for drag, lift, and pitch while in the water tunnel. Also, before the experiments, the pressure gages were calibrated first in air then in water. During the experiments, pressure gage calibrations were re-checked several times using the water tunnel as a reference. After the experiments, dynamometer and pressure gage calibrations were re-checked. Both pressure and force gage calibrations were quite linear. Accuracy for both pressure and force gages is typically $\pm 0.5\%$ of the full scale deflection. This is interpreted as an error band of $\pm .1$ psi for pressure and ± 2 lbs. for force measurements.

DATA REDUCTION AND ANALYSIS

This section presents a brief discussion of the methods employed to evaluate the experimental data. Items covered are the measurements that were made, the analysis of force data, the analysis of pressure data and the calculation of the model pressure recovery.

The measurements made include:

the water tunnel test section velocity

the water tunnel test section ambient pressure

the shaft speed of the pump

the flow rate through the model

the drag, lift, and side forces acting on the model

the yaw, pitch, and roll moments acting on the model

the external axial static pressure distribution on the inlet lip

the external peripheral static pressure distribution on the inlet lip

the static pressure profile in the lower strut after the vaned turn

the total pressure profile in the lower strut after the vaned turn

the static pressure profile at the top of the strut

the total pressure profile at the top of the strut

the static pressures at the transition piece.

The calculated quantities from the data reduction program used for analysis of pressure data (Appendix D) are:

1. inlet velocity, V_{IN}, based on actual inlet area

2. the inlet velocity ratio, IVR, based on actual area and also based on the cruise configuration inlet area

3. the pressure coefficient, C_p, from measurements.

$$C_p = (P - P_\infty)/ (1/2)\rho(V_\infty)^2$$

4. the pressure coefficient, C_p, for internal pressure measurements

$$C_{P_I} = (P - P_\infty)/(1/2)\rho(V_i)^2$$

5. the average static pressure after the vaned turn

6. the average total pressure after the vaned turn

7. the average static pressure at the strut exit

8. the average total pressure at the strut extit

9. the free stream total pressure

$$P_{T_\infty} = P_\infty + (1/2)\rho(V_\infty)^2$$

10. the local inlet pressure from Bernoulli's equation

$$P_{(in)} = P_{T_\infty} - (1/2)\rho(V_{in})^2$$

11. the local cavitation number

$$\frac{P_{in} - P_v}{(1/2)\rho(V_{in})^2}$$

12. the inlet Reynolds number

$$R_{e(in)} = \frac{V_{in} \text{ X Diameter}}{\gamma}$$

13. the pressure loss coefficient, computed by the area average method; based on free stream speed

$$\frac{P_{T_\infty} - P_{T\text{ (strut exit)}}}{(1/2)\rho(V_\infty)^2}$$

and based on inlet velocity

$$\frac{P_{T_\infty} - P_{T\text{ (strut exit)}}}{(1/2)\rho(V_I)^2}$$

where $P_{T\text{ (strut exit)}}$ is the area-average total pressure at the strut exit.

The forces and moments acting on the model are analyzed in the following manner. The response of the dynamometer's six block gages is multiplied by the six by six matrix of calibration coefficients. This produces the combination of forces and moments that act on the model. The matrix of calibration coefficients accounts for the response of all the gages due to any loading. It accounts for both the response of the primary loaded gage or gages and the response of a gage under interaction loading. This interaction type of loading is usually caused by mechanical interference and the deflection of components within the dynamometer.

The force and moment are then further reduced in the usual manner. Forces are expressed in coefficient form, i.e., Force Coefficient, $C_F = \text{Force}/(1/2)\rho S V_\infty^2$

The reference area, S, is the estimated total wetted area of the strut-pod model. More precisely, the wetted area S refers to the sum of 1) the pod external wetted area from the lip to the blunt base, base area not included, and 2) the strut external wetted area from leading edge to the blunt base and from the strut-pod intersection up to a strut height selected to be the upper bound of the strut which was in the presence of the tunnel flow stream.

Other calculated values include:

the inlet momentum $MO = \rho\ Q\ V_{in}$

the inlet momentum drag coefficient

$$C_{D_{mo}} = \frac{\rho\, Q\, V_{in}}{(1/2)\rho\, S\, V_\infty^2}$$

the external drag, $\text{Drag}_{(ex)}$ = Measured Drag-(Momentum Drag+Inlet Pressure)

the external drag coefficient, $C_{D_{(ex)}} = \dfrac{\text{Drag}_{(ex)}}{(1/2)\,\rho\, S\, V_\infty^{\,2}}$

the inlet pressure force, P. force $= (P_i - P_\infty) \times A_i$

the inlet pressure drag coefficient, $C_{D_P} = \dfrac{(P_i - P_\infty) \times A_i}{(1/2)\,\rho\, S\, V_\infty^{\,2}}$

and, similar quantities for the model lift forces.

A listing of the data reduction computer program used for the force analysis is given in Appendix E.

PRESENTATION AND DISCUSSION OF EXPERIMENTAL RESULTS

PRESSURE MEASUREMENTS

Centerbody Axial Pressure Distribution:

The nondimensional pressure coefficients were plotted versus axial distance along the centerbody. The full complement of such data for all experimental conditions are to be presented in an addendum to this report. Some of the data have been extracted and are included here for comparative purposes.

Figure 5 presents the comparison of measured data with the prediction for: prototype velocity of 80.45 knots, IVR $(Q/A_{i_c} \cdot V_\infty) = 0.71$, and centerbody fully extended. The experimental data are in relatively good agreement with the prediction. Data for other IVR values are not shown because, as expected, changing IVR has no significant effect on the centerbody pressure distribution for the fully extended centerbody.

Figure 6 presents the comparison of measured data with the prediction for: prototype velocity = 9.85 knots, IVR $(Q/A_{i_c} \cdot V_\infty) = 3.34$, and centerbody fully retracted. Experimental data are given for IVR = 2.8, 3.2, and 3.4. The comparison shows that the predicted C_p for IVR = 3.34 is approximately equal to that measured for IVR = 3.2. This indicates that, if the measurements are correct, the analytical technique underpredicts the minimum pressure coefficient on the centerbody for the fully retracted position. Note that, as expected, for the fully retracted centerbody, its pressure distritution is sensitive to IVR changes.

Inlet Lip - External Axial Pressure Distribution:

Pressure coefficients, computed from experimental data, are plotted versus axial distance along the exterior surface of the inlet lip. Again the bulk of this data will be included in the addendum to this report.

Figure 7 presents the measured C_p pressure distribution versus axial distance from the leading edge of the inlet lip for conditions of: simulated speed = 100 knots, centerbody fully extended, and several IVRs. The typical change in external pressure distribution with varying IVR is shown; i.e., the reduction of $C_{p_{min}}$ with decreasing IVR. Also shown is that, when $C_{p_{min}} = -\sigma$ (local pressure coefficient equal to the negative value of the ambient cavitation number) then cavitation occurs and $C_{p_{min}}$ cannot be reduced further. This was verified by observation during the experiment; i.e., no cavitation was observed for runs 197 through 200, whereas for run 201 a cavity (approx. 2 inches long) was observed as is indicated by the data.

Strut Internal Pressure Distribution:

Internal flow pressure distributions (presented as measured pressure in psia versus distance from the leading edge of the strut internal flow area) are shown in Figures 8A and B for the upper and lower strut measurement planes respectively. (See Figure 3 for location of the measurement planes.) Both figures are for test conditions of: fully retracted centerbody, simulated

pre-take-off (35 knots/ 18 ft submersion), and several IVRs ($IVR = Q/A_{i_c} V_\infty$). Figure 8A indicates 1) a fairly uniform total pressure distribution with a non-uniform static pressure distribution along the length (low static pressure in the forward portion of the flow area), 2) the general decrease in pressure with high IVR (high flow rate), and 3) the very low pressures and non-uniform profiles associated with internal cavitating conditions (runs 121 and 122). Figure 8B (measurement plane just beyond the vaned turn) indicates non-uniform total and static pressure distributions, and, similar to 8A, the general decrease in pressure with high IVR and the low, non-uniform pressure profiles associated with cavitating conditions.

The flow velocity is related to the difference in total and static pressure, $V \sim \sqrt{\frac{2(P_T - P_S)}{\rho}}$. As such, the flow velocity distribution within the strut could be deduced from an extensive pressure survey. It was felt by the investigators that the pressure survey taken was inadequate for the performance of velocity calculations but that qualitative information about the velocity profile can be deduced.

For moderate IVRs, Figure 8B indicates (qualitatively) a region of relatively high velocity for 1 inch $< X <$ 4 inches, relatively low velocity for $4 < X < 6$, high velocity for $6 < X < 12$, and low velocity or possibly reverse flow for $X >$ 12 inches. At the top of the strut, Figure 8A indicates high velocity in the forward region and moderate to low velocity in the rearward region of the flow

area. In general, a poor flow distribution is indicated, probably due to the centerbody/vaned turn system. For cavitating conditions, regions of high velocity far forward and far rearward are indicated in the flow area just beyond the vaned turn. Also, high velocity is indicated in the rearward portion of the flow area at the top of the strut.

PRESSURE RECOVERY PERFORMANCE

The pressure recovery performance of the inlet-diffuser presented as a pressure loss coefficient is shown in Figure 9 for centerbody positions of 30.73 and 34.73 inch extensions and simulated speeds of 80 and 100 knots. At the design IVR = 0.85, the pressure loss coefficient is approximately $C_{P_L} = 0.25$. This value, scaled up to a value for the prototype would become $C_{P_L} \sim 0.23$ to 0.24. This value compares to the predicted $C_{P_L} = 0.242$. As such, the prediction and model data are in good agreement. Also, as indicated in the design report (Reference 10), this value satisfies the pressure recovery requirements for the inlet at its high speed operating condition.

The sharp upward trend of the pressure loss coefficient, at high IVR, is indicative of inlet internal cavitating conditions.

Note that the above loss coefficients do not represent the pressure loss up to the pump inlet but only the loss up to about 75% of the total strut height. For an estimate of loss up to the pump inlet, one would have to increase C_{P_L} by 0.1 to 0.3 depending on duct length, number of flow turns, and pump position.

To scale the pressure loss up to a prototype value, one should account for both the form and friction losses. Typically, the form loss coefficient depends on the shape or the goemetry of the duct and it is assumed that model C_{P_L} (form) = prototype C_{P_L} (form) for a geometrically similar model. The friction loss coefficient does depend on the actual size, velocity and ambient turbulence level; that is, the friction loss coefficient is Reynolds number dependent. The scaling of friction loss coefficient should account for the change in Reynolds number from model to prototype. For this investigation, the accurate differentiation between friction and form losses of the inlet-diffuser is a near impossible task. As such, the scaled prototype C_{P_L} should be considered as an estimate.

The pressure loss coefficients for the model at low speed conditions (i.e., centerbody fully retracted and simulated speeds of 20 and 35 knots full scale) are presented in Figure 10. Rather high losses are indicated. At the hump-speed design IVR = 2.35 (based on cruise inlet area) or IVR = 0.89 (based on actual inlet area), the value of the model pressure loss coefficient, C_{P_L}, is 1.60. Such losses are indicative of internal cavitating conditions. Also, this value greatly exceeds the predicted C_{P_L} = 0.282. From this data, we may conclude that the inlet design will not provide the required performance at the hump speed.

One should now examine the internal performance of the inlet model throughout it's variable-area range. This is presented in Figure 11 as pressure loss coefficient versus IVR for each centerbody position as tested. All data is for the water tunnel test condition which

simulates the 35 knot post take-off. Note that there are two IVR definitions used. These are; IVR based on cruise inlet area for the left hand graph, and IVR based on actual inlet area for the right hand graph. Since all the data are at one test condition (one value of free stream velocity), the IVR (left hand graph) is proportional to flow rate ingested and the IVR (right hand graph) is proportional to the inlet velocity.

The left hand figure shows that as the centerbody is retracted the inlet flow limit (the sharp upward trend) does move to higher IVR (flow rate). Certainly, this is expected.

The right hand figure shows that the flow limiting IVR or maximum inlet velocity also varies with centerbody position. For the centerbody fully extended 34.73 inch, the flow limiting IVR is approximately 1.1 (i.e. inlet velocity = 110% free stream). For intermediate centerbody positions, the flow limiting IVR is rather high; 130% to 150% of the free stream. But for the fully retracted centerbody, the limiting inlet velocity is only 80% of the free stream. This indicates a poor ability to accomodate high inlet velocities for the centerbody-retracted configuration of the inlet design.

CAVITATION PERFORMANCE

The inlet cavitation inception boundaries for the cruise configuration (centerbody fully extended) are shown in Figure 12. For this configuration, cavitation was found to occur on the inner and

outer surfaces of the inlet lip near the leading edge; no cavitation was observed on the centerbody. The data indicate that the inlet design meets its flow rate requirement at 100 knots. The ΔIVR margin to cavitation is respectable. The experimental data and prediction for external cavitation are in good agreement. The data for internal cavitation indicate a higher IVR attainable than predicted.

At simulated high speeds, 80 knots or better, cavitation was observed at the strut-pod intersection. Refinement of the strut-pod fairing shape will be required.

Photographs of representative cavitating conditions for the inlet's cruise configuration are shown in Figure 13.

The inlet cavitation inception boundaries for the centerbody extension of 24.44 inch full scale are presented in Figure 14. For this configuration, inception of external cavitation occurred at the lip leading edge, while internal cavitation occurred at the minimum area or throat region on either the centerbody or the inner surface of the inlet lip. Agreement between data and the predictions is poor.

Photographs of typical inlet cavitating conditions for centerbody extension of 24.44 inch full scale are shown in Figure 15.

The inlet cavitation inception boundaries for the centerbody extension of 15.0 inch full scale are presented in Figure 16. External cavitation inception was observed at the inlet lip leading edge. Internal cavitation was located at the minimum area (throat) region. Again, internal cavitation was observed on either the centerbody or lip surfaces. Agreement between data and the prediction is lacking. The inlet, in this configuration, cannot operate cavitation free at

speeds in excess of 65 knots.

The inlet cavitation inception boundaries for the centerbody fully retracted configuration are presented in Figure 17. Cavitation inception, both internal and external, did occur at the inlet lip leading edge. At conditions simulating 35 knots - 18 ft. submersion, the model data indicate internal cavitation inception at an IVR = 2.32 and maximum or choked flow at an IVR = 2.42. At conditions simulating 35 knots - 4 ft. submergence, the model data indicate internal cavitation inception at an IVR = 2.15 and choked flow at an IVR ≈ 2.20. These values are significantly less than those predicted. Also, they are such that the IVR = 2.35 required to accelerate the craft through hump would probably not be sustained as the craft rises.

Photographs of typical inlet cavitating conditions for the centerbody fully retracted configuration are shown in Figure 18.

Further development of the inlet lip shape or possible further retraction of the centerbody might improve the resistance to internal cavitation.

DRAG PERFORMANCE

Figure 19 presents the typical inlet drag performance for a range of IVR values. Two sets of data are shown; 19A is for the inlet with centerbody fully retracted at σ = 2.833 simulating 20 knots full scale, 19B is for the inlet with centerbody fully extended at σ = 0.082 simulating 100 knots full scale. Shown are the total measured drag, the inlet momentum drag, the inlet pressure drag, and the computed external drag. Total measured drag is equal to the sum of x - direction forces acting on the model reacted by the dynamometer. Inlet momentum

drag is the x - direction force equal to the actual pressure at the inlet plane less the ambient pressure multiplied by the inlet area. It is the pressure or suction force at the inlet due to pre-diffusion or pre-contraction of the ingested flow. The computed external drag is equal to the measured drag less the flow related forces of inlet momentum and inlet pressure. It is thus a measure of the external friction and form drag acting on the pod-strut body. As shown in Figure 19, the strut-pod external drag is relatively insensitive to changes in IVR. The significant drag forces associated with an operating inlet are the inlet momentum drag and the inlet pressure drag; the change in the external drag force associated with an operating inlet is of secondary importance.

Strut-pod drag performance versus cavitation number is presented in Figure 20. Shown are drag coefficients for the strut-pod with solid nosepiece fairing over the inlet compared with coefficients of calculated external drag for the strut pod (inlet operating) of both fully extended and fully retracted centerbody configurations. The data indicate that the external drag of the strut-pod with operating inlet is approximately equal to the external drag of the strut-pod with solid nosepiece.

No comparisons of predicted drag with experimental results have been made. The predictions that were made had only accounted for friction drag on the axisymmetric pod for several different tail options. A first effort has been made to reduce the strut-pod drag into components of strut friction drag, strut pressure drag, pod friction drag, pod pressure drag, and strut-pod interference. This

first analysis was halted because of some complications and no results are available for presentation in this report. Further analysis of the strut-pod drag is underway. The results of which will be published in a follow-on report.

CONCLUSIONS

1. The model experiments demonstrated that the variable-area inlet in its cruise configuration at 0° yaw and 0° pitch is capable of 100 knots (51.44 m/s) cavitation free operation, in undisturbed flow.

2. Predicted pressure distribution and cavitation boundaries for the inlet in the cruise configuration are in good agreement with the data. The prediction for the inception of internal cavitation is conservative.

3. At simulated take-off conditions, the model with centerbody fully retracted could not accomodate the required flow rate without cavitation. At a simulated 35 knots (18 m/s) and 18 ft. (5.5 m) submergence, the inlet operates with partial cavitation at the required flow rate. At a simulated 35 knots (18 m/s) and 4 ft. (1.22 m) submergence, the inlet chokes at IVR = 2.20 and the required flow rate cannot be attained. The prediction of a cavitation-margin ΔIVR = 0.2 for the required IVR = 2.35 was not realized.

4. The prediction of cavitation inception boundaries for all off-design centerbody positions are not in agreement with the model data.

5. At off-design centerbody positions of 15 inch (0.38 m) and 24.44 inch (0.62 m) extension (full scale), the internal cavitation

was found to occur at the minimum-area (throat) region. This is in contrast with the prediction that internal cavitation would be located at the inlet lip leading edge for all centerbody positions.

6. Pressure recovery performance of the model for the centerbody fully extended configuration agree with the prediction. For the centerbody retracted configuration, the performance is relatively poor and does not agree with predictions.

7. The drag performance of the operating waterjet inlet is found to be highly dependent on the ingested flow related forces of inlet momentum and inlet pressure. Variations in the external (form and friction) drag of the pod-strut body due to the operating inlet are small.

RECOMMENDATIONS

1. Other analytical techniques for the prediction of inlet pressure distribution and cavitation inception boundaries should be investigated. The capability of the presently used technique to predict inlet performance, particularly for off-design centerbody deployments, is limited.

2. To improve the cavitation performance of the variable-area inlet design, it is recommended to; (a) reduce the constriction at the inlet minimum area (throat) region, (b) increase the inlet lip nose radius, and (c) reconsider the limits of travel of the centerbody to assure minimal interference of the centerbody with the inlet flow during full retracted operation. The effects of these suggested design changes should be evaluated on an analytical basis with the use of available design and performance prediction techniques. If

the results appear promising, an experimental evaluation of the modified design should be conducted.

3. Redesign of the centerbody-turning vane should improve internal pressure recovery performance.

4. A comparison of the performance of this variable-area inlet and a fixed-area inlet is currently underway. Drag, cavitation, and pressure recovery performance of the inlets for a given flow-rate/speed schedule will be compared.

5. Due to funding limitations, the sensitivity of this design to pitch or Yaw angle was not investigated. This aspect would be important to explore. The ability to deliver the required thrust in a turn, during maneuvers, or in a seaway is an essential aspect for satisfactory prototype ship performance.

REFERENCES

1. Sherman, Peter M., and Lincoln, Frank W., "Ram Inlet Systems for Waterjet Propulsors, AIAA Paper No. 69-418, May 1969

2. Levy, J., "The Design of Waterjet Propulsion Systems for Hydrofoil Craft," Presented to SNAME Southern California Section, May 1964

3. Hatte, R., and Davis, H.J., "Selection of Hydrofoil Waterjet Propulsion Systems," AIAA Paper No. 66-732, August 1966

4. Johnson, Virgil E. Jr., "Waterjet Propulsion for High Speed Hydrofoil Craft," AIAA Paper No. 64-306, July 1964

5. Arcand, L., and Comolli, D.R., "Waterjet Propulsion for High Speed Ships," AIAA Paper No. 67-350, May 1967

6. Brandau, John H., "Aspects of Performance Evaluation of Waterjet Propulsion Systems and a Critical Review of the State-of-the-Art," AIAA Paper No. 67-360, May 1967

7. Wislicenus, George F., "Hydrodynamic Design Principles of Pumps and Ducting for Waterjet Propulsion," DTNSRDC Report 3990, June 1973

8. Barr, R.A. and Stard, N.R., "Current State-of-the-Art of Waterjet Inlet Systems for High Performance Naval Ships," Hydronautics, Incorporated Technical Report 7244-5, December 1973

9. Barr, R.A., and Etter, R.J., "Selection of Propulsion Systems for High Speed Advanced Marine Vehicles," AIAA/SNAME Advanced Marine Vehicles Conference, February 1974

10. Developmental Sciences Inc., "Design of a Pod Inlet for a 200 Ton, 100 Knot Hydrofoil," Aerospace Technology Division, November 1973

11. Callanen, Stephen, "A New Experimental Facility for the Performance Evaluation of Strut-Pod Waterjet Inlets at Cavitation Scaled Craft Speeds in Excess of 100 Knots," DTNSRDC Ship Performance Department Report, SPD-671-01, December 1975

12. Brownell, W.F., "A 36-Inch Variable Pressure Water Tunnel," DTNSRDC Report 1052, June 1956

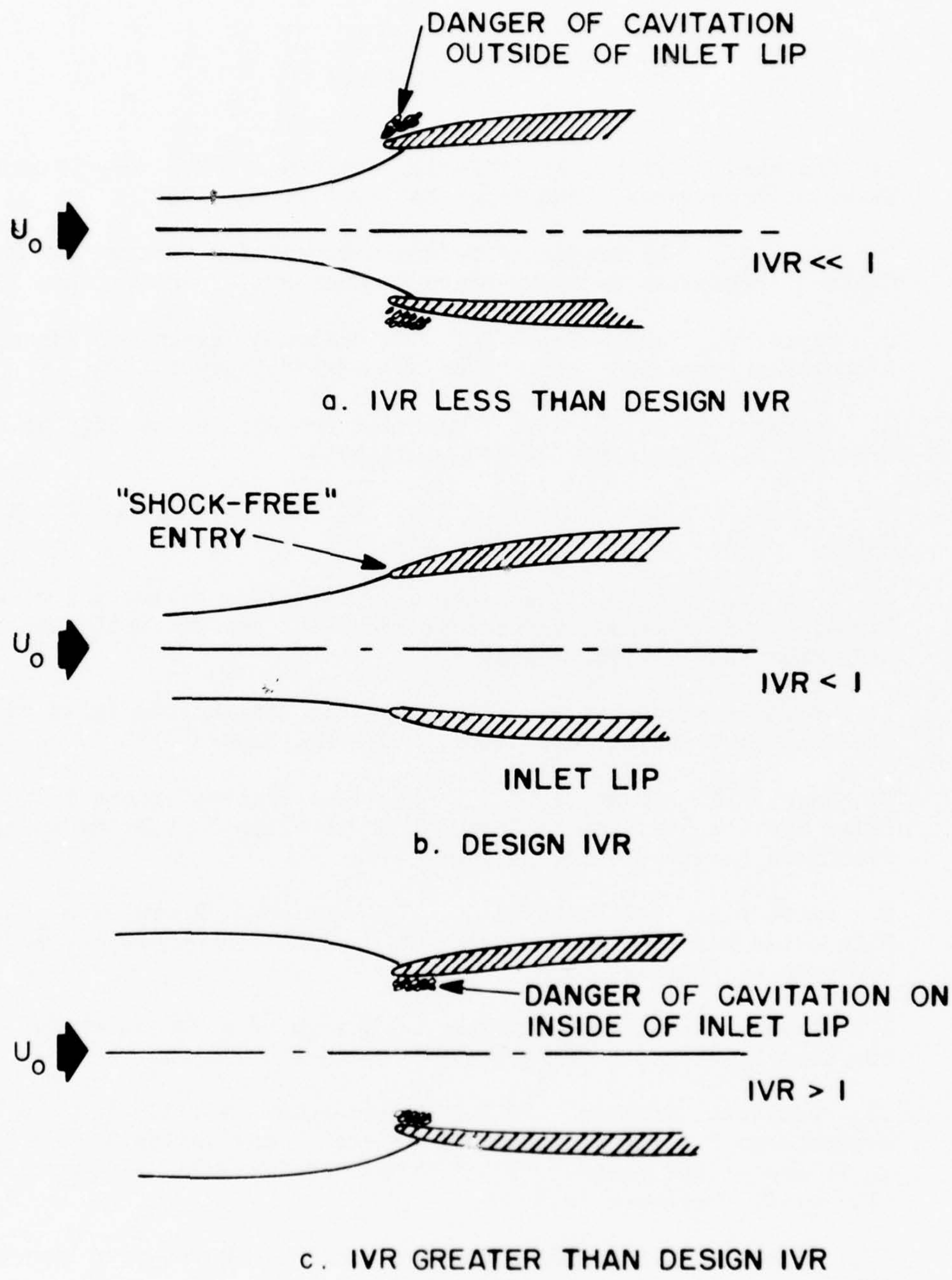

Fig. 1 Variation of Inflow Angle With Inlet Velocity Ratio (IVR) For A Typical Inlet

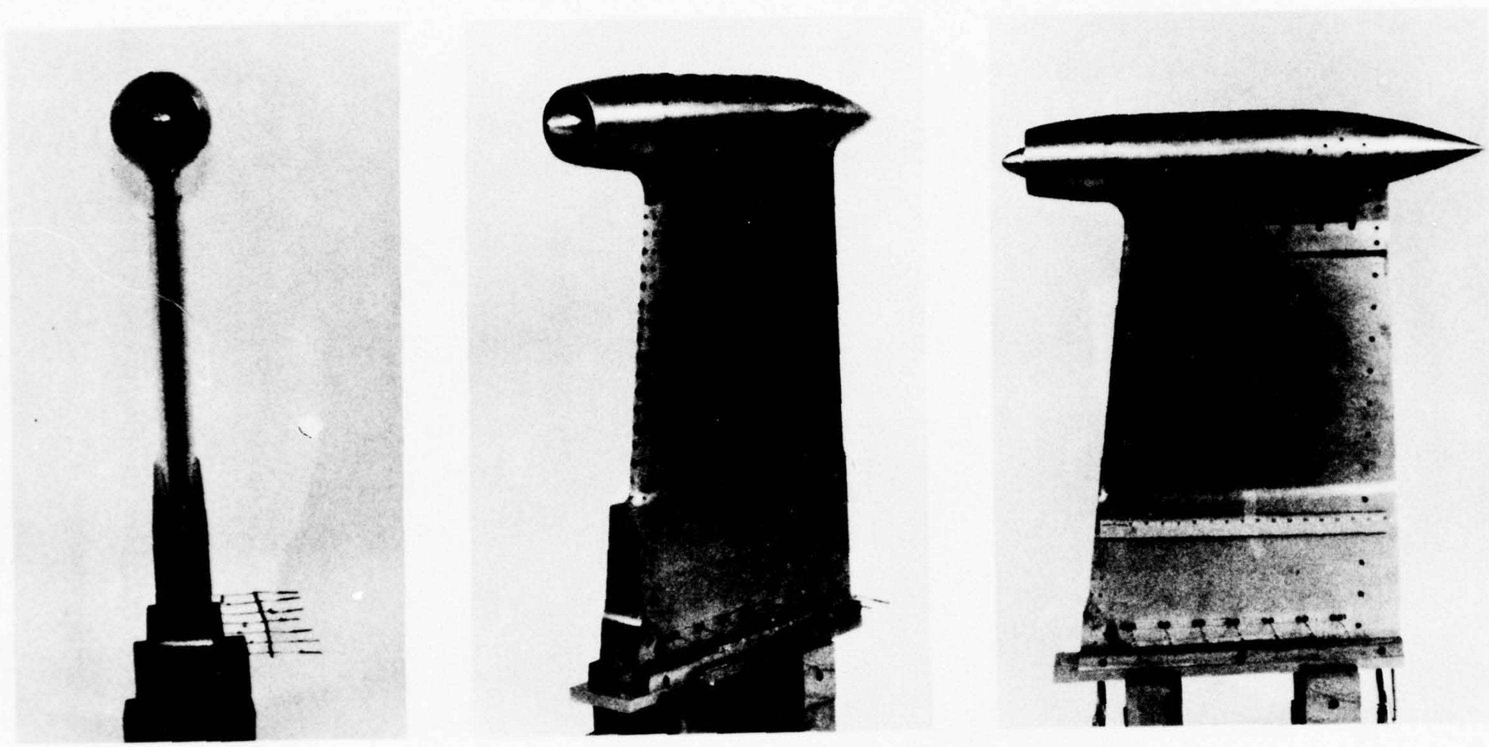

Figure 2A- Photographs of Strut-Pod Model and Associated Components

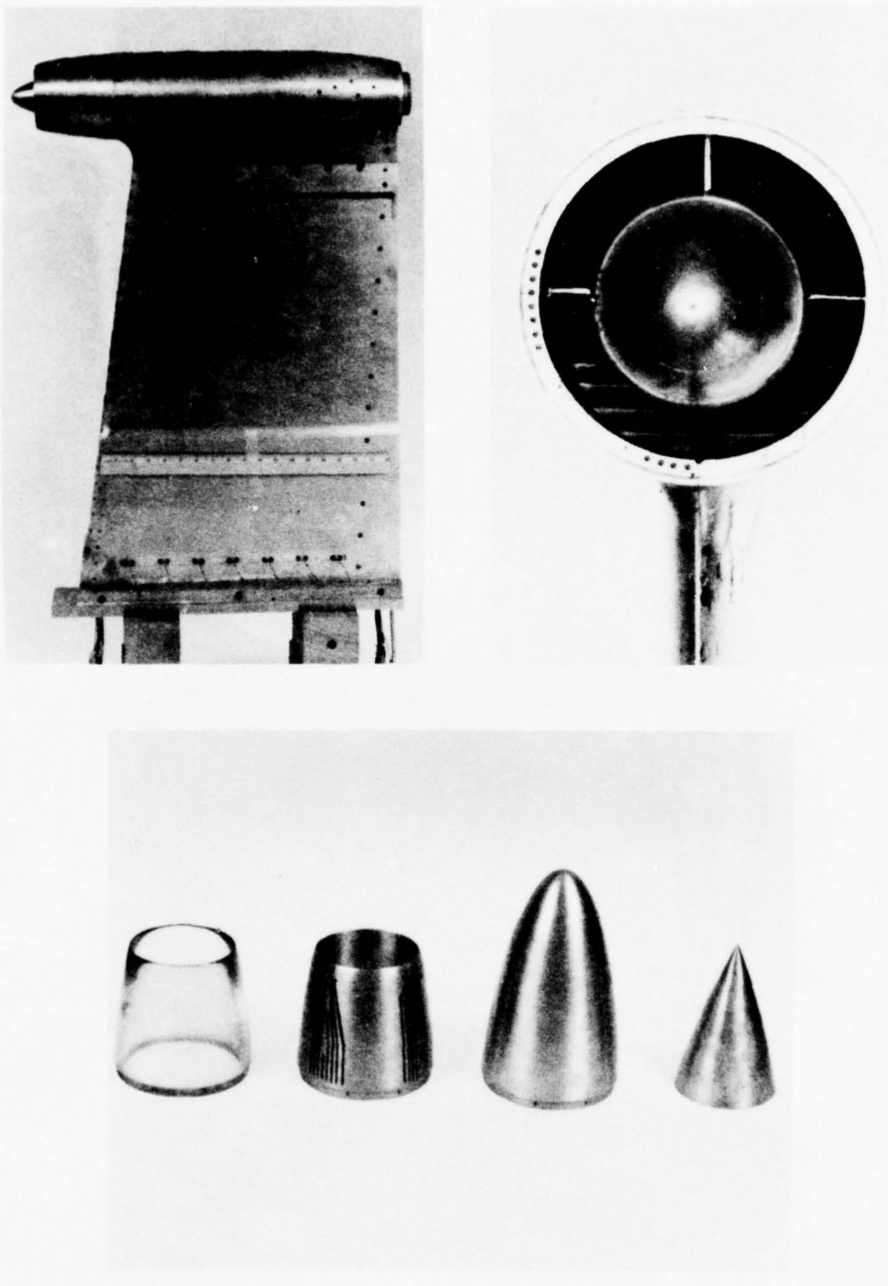

Figure 2B—Photographs of Strut—Pod Model and Associated Components

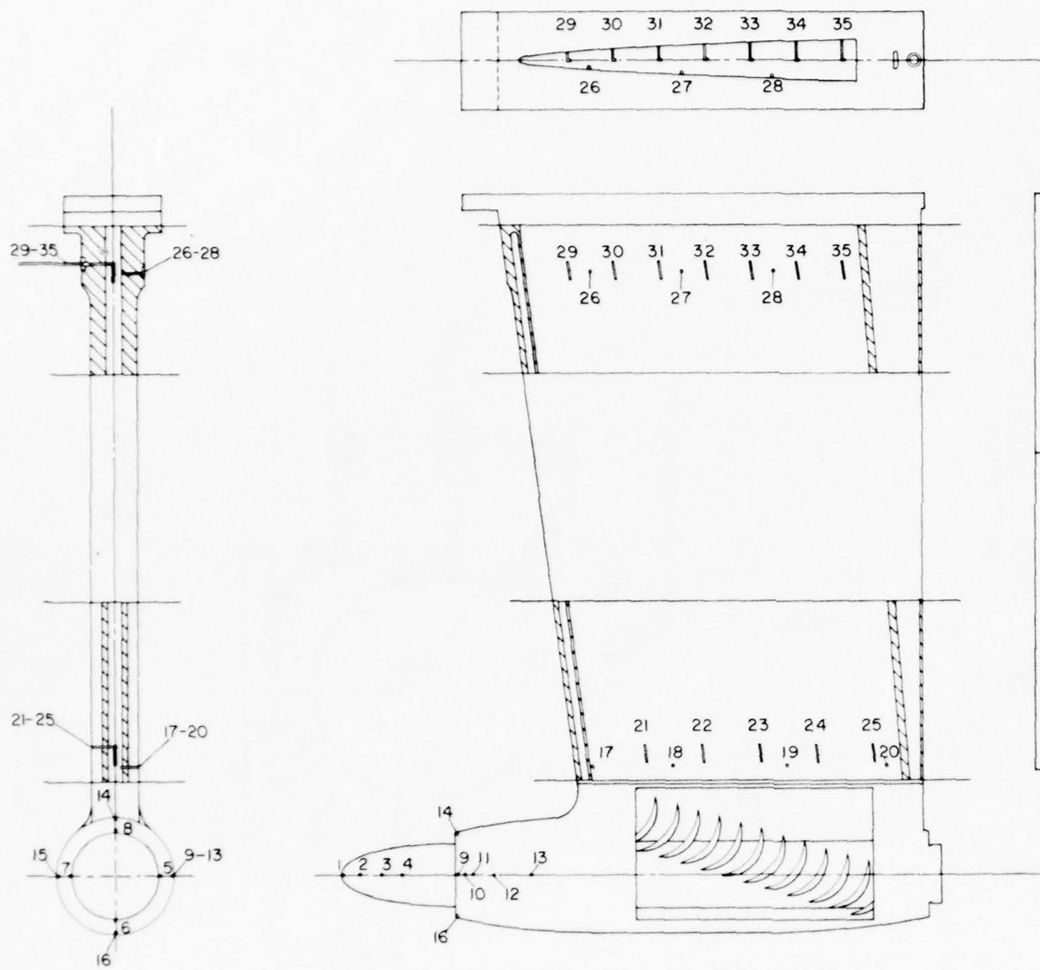

PRESSURE TAP LOCATIONS X-DISTANCE FROM LEADING EDGE			
LIP		CENTER BODY	
PROBE	X	PROBE	X
9	0.100	1	0
5,6,7,8,10	0.450	2	0.890
11,14,15,16	0.850	3	1.890
12	1.850	4	2.890
13	3.600		
LOWER STRUT		TOP OF STRUT	
PROBE	X	PROBE	X
17	0	26	4.080
18	3.720	27	8.150
19	7.440	28	12.230
20	11.160	29	2.070
21	2.750	30	4.250
22	5.470	31	6.430
23	8.190	32	8.610
24	10.910	33	10.790
25	13.630	34	12.970
		35	15.150

Figure 3 Sketch of Model-Pressure Probe Locations

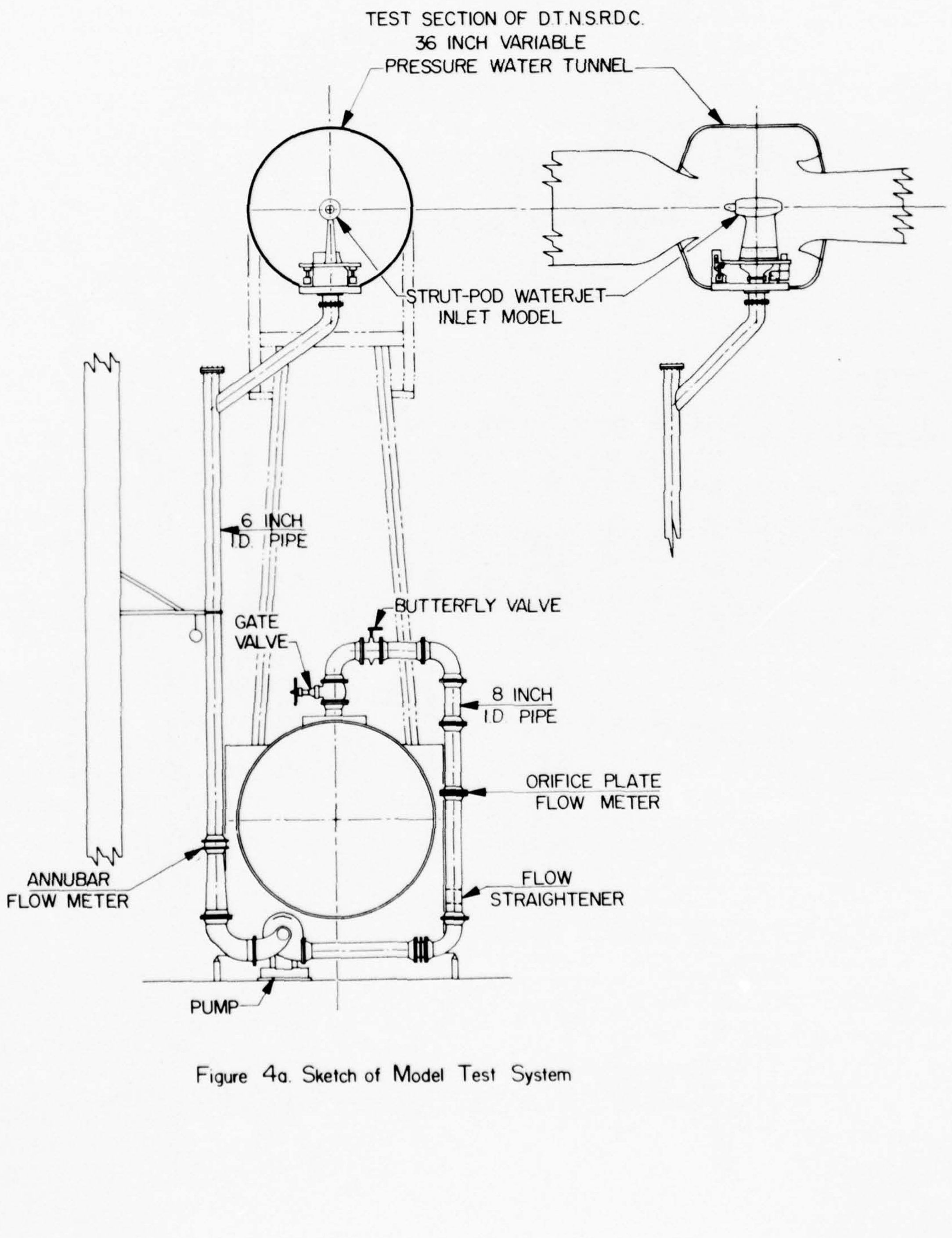

Figure 4a. Sketch of Model Test System

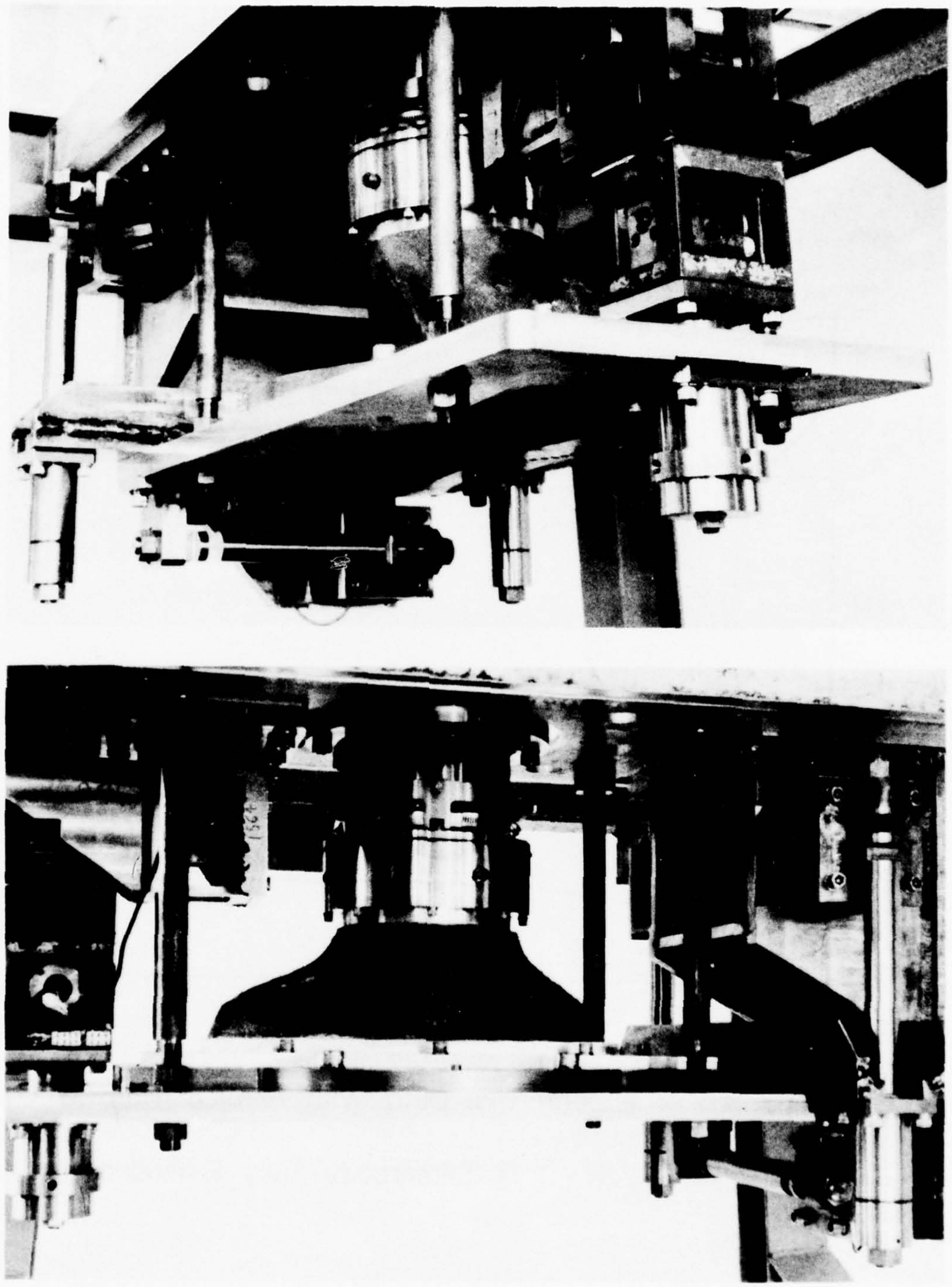

Figure 4B–Photographs of 6-Component Dynamometer

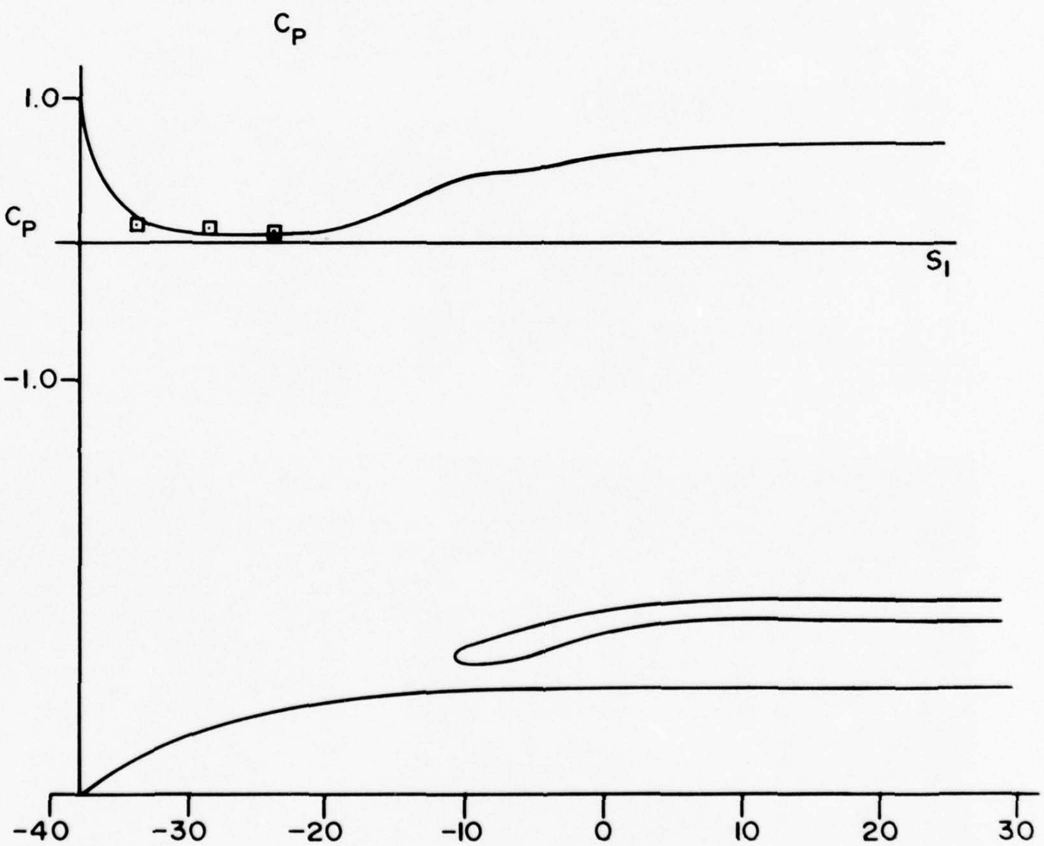

Fig. 5 Comparison of Experimental Data With Prediction of Centerbody Pressure Distribution.
V = 80.45 kts, IVR = 0.71, Centerbody Fully Extended

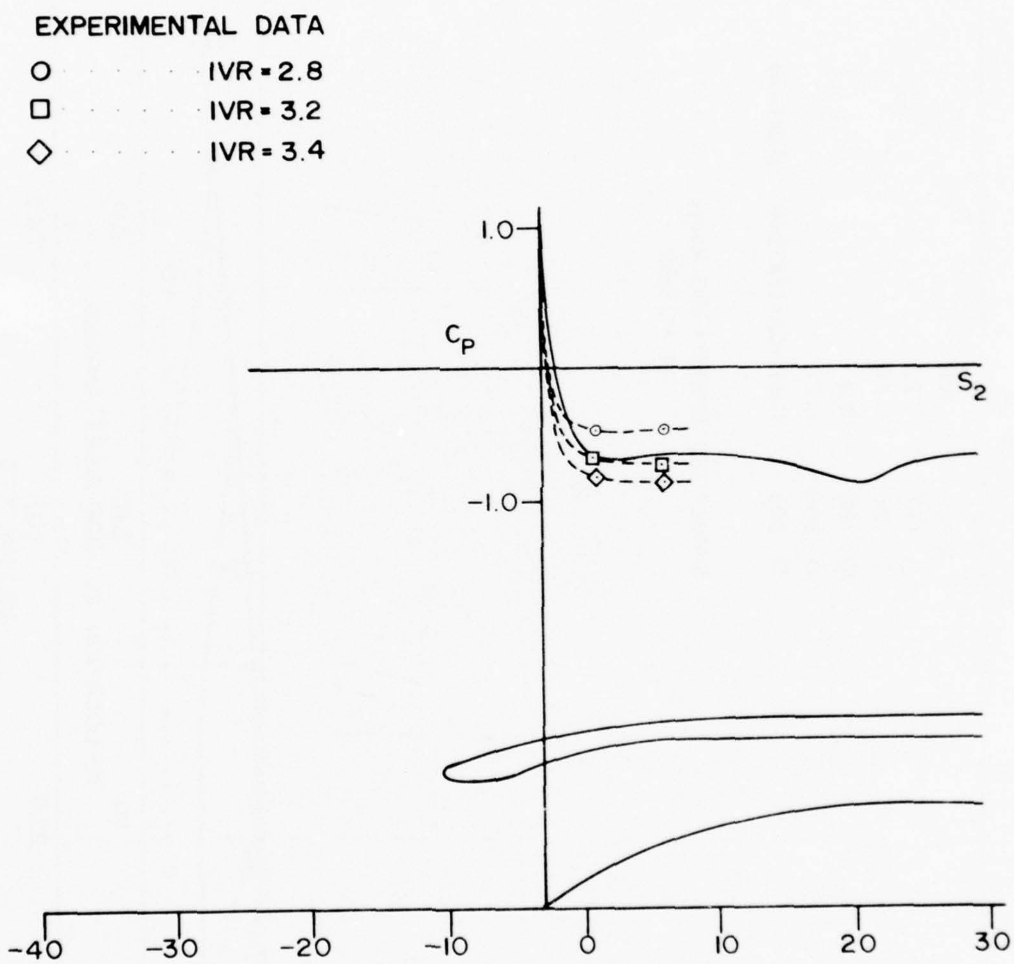

Fig. 6 Comparison of Experimental Data With Prediction of Centerbody Pressure Distribution.
V = 9.85 kts, IVR = 3.34, Centerbody Fully Retracted

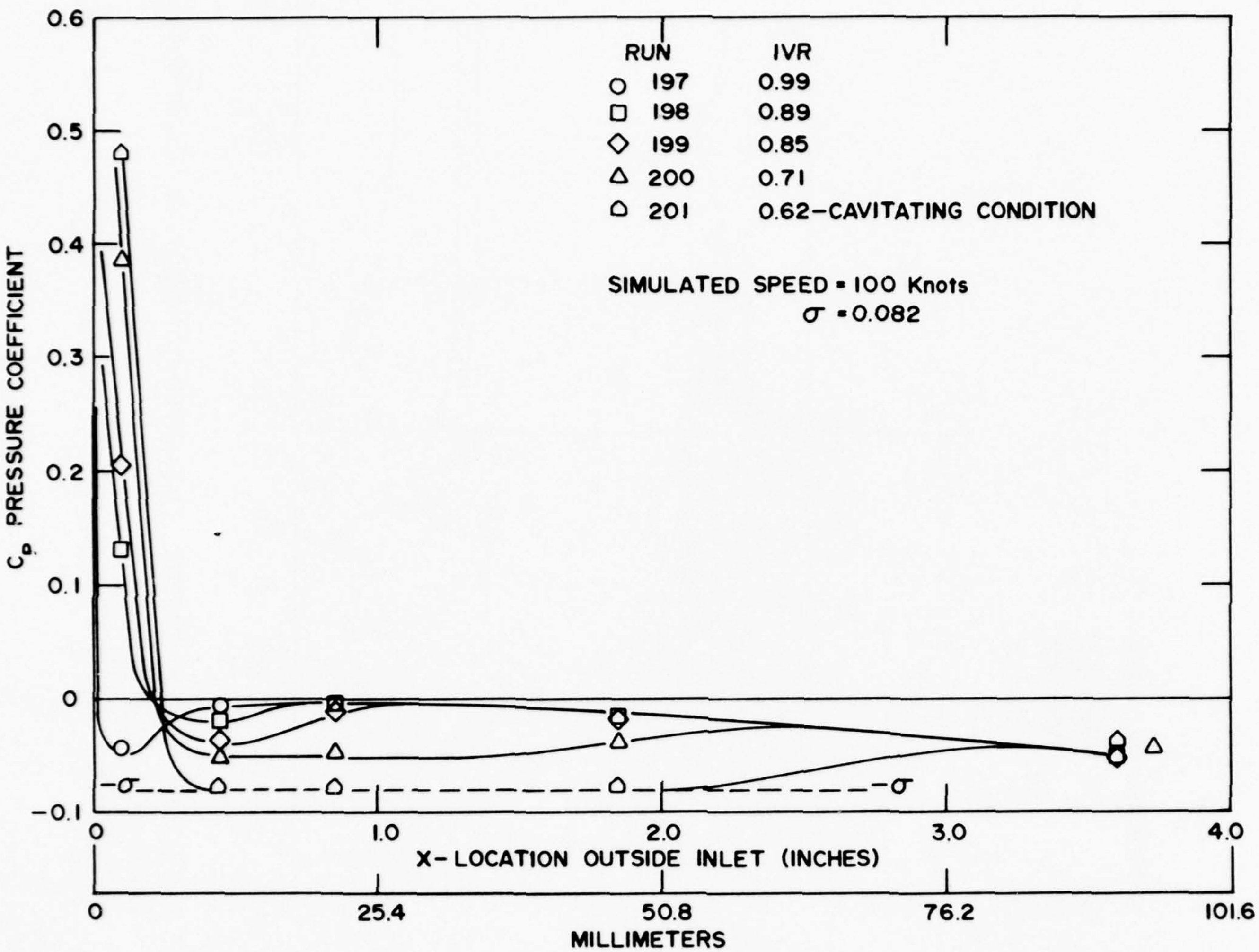

Figure 7. Experimentally Determined Axial Pressure Distribution on the Exterior Surface of the Inlet Lip for a Simulated Speed of 100 Knots (51.4 m/s) and Several IVR Values.

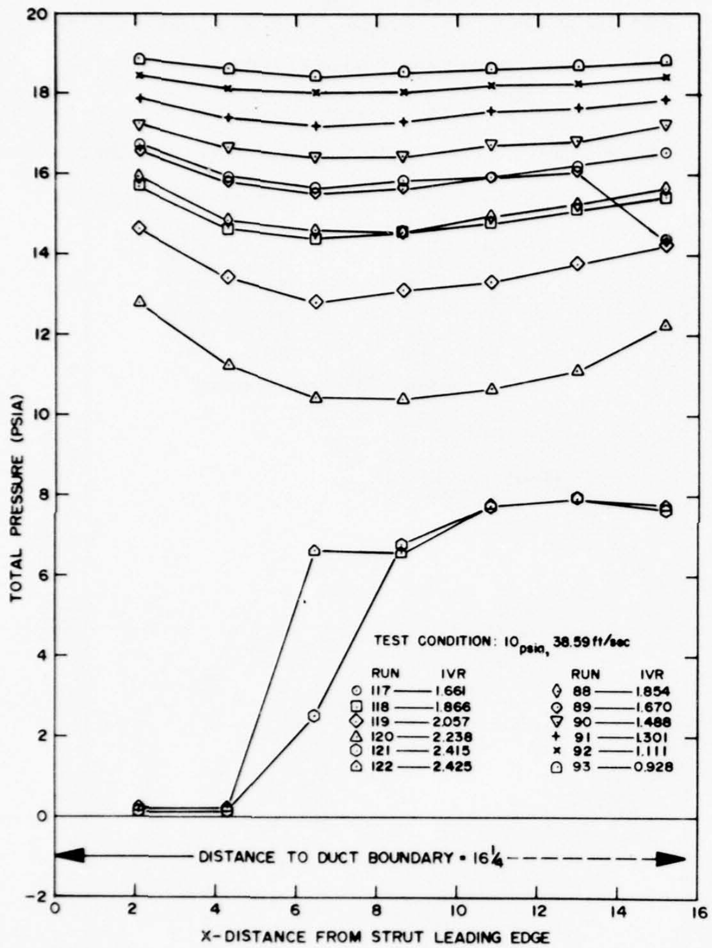

Figure 8a. Internal Pressure Distribution at the Top of the Strut
(TOTAL PRESSURE)

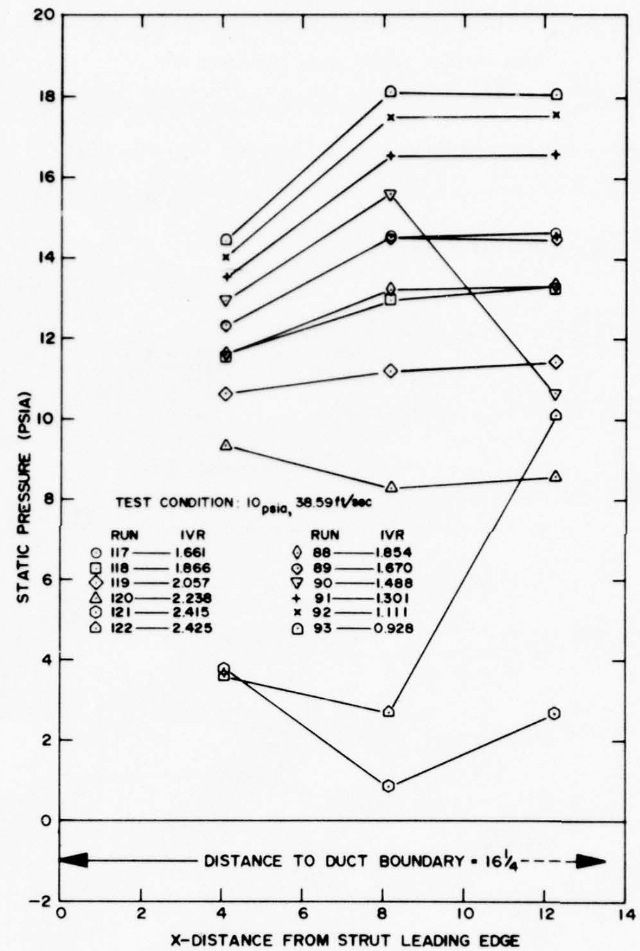

Figure 8a. Internal Pressure Distribution at the Top of the Strut
(STATIC PRESSURE)

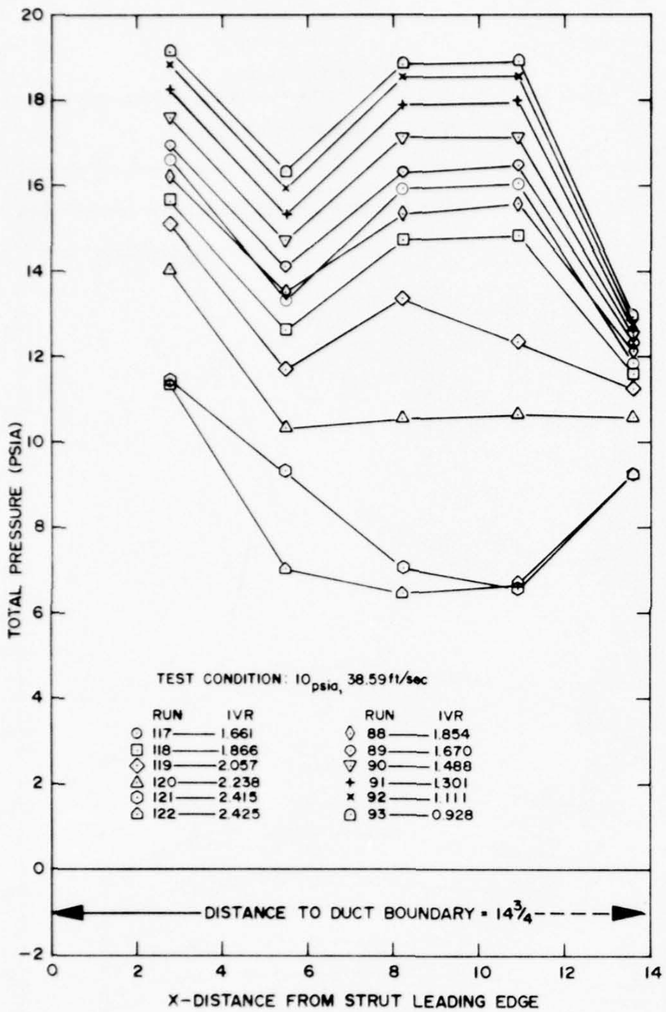

Figure 8b Internal Pressure Distribution at Bottom of the Strut
(TOTAL PRESSURE)

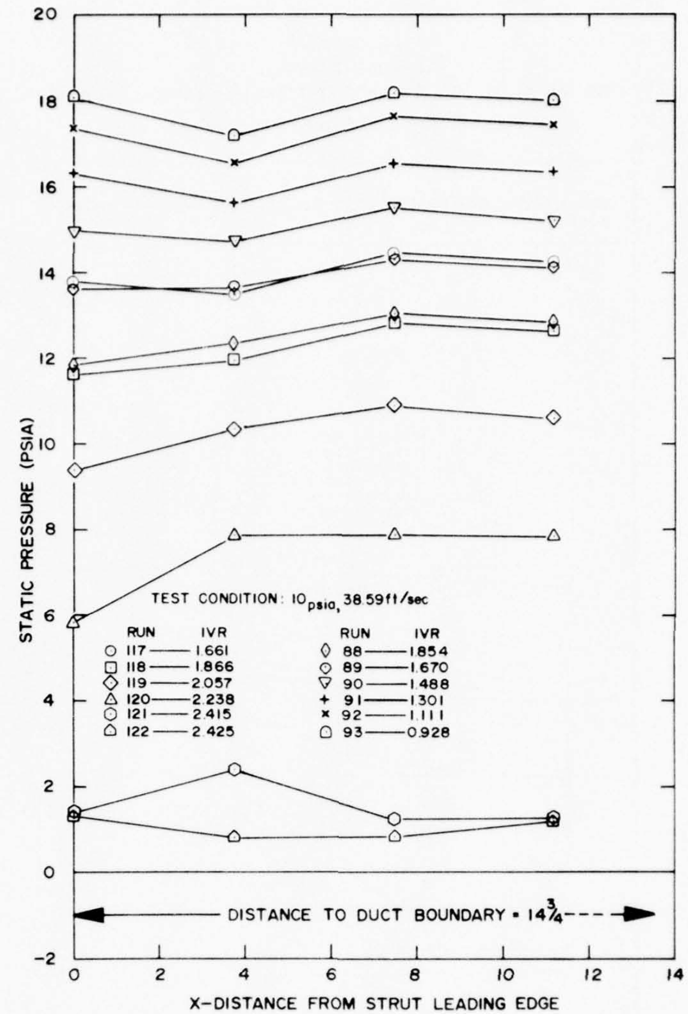

Figure 8b Internal Pressure Distribution at Bottom of the Strut
(STATIC PRESSURE)

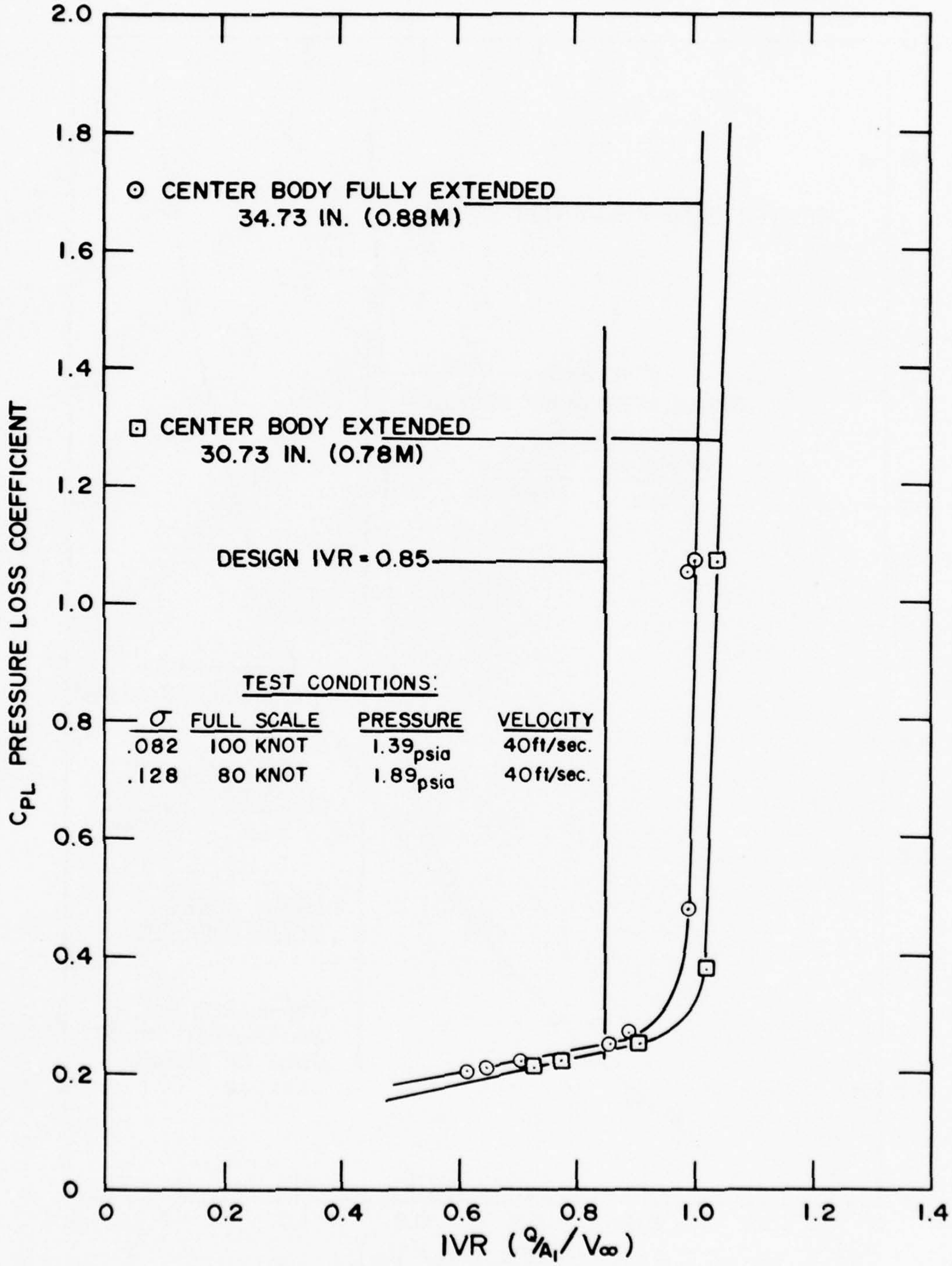

Figure 9. Internal Pressure Loss Performance—High Speed Conditions.

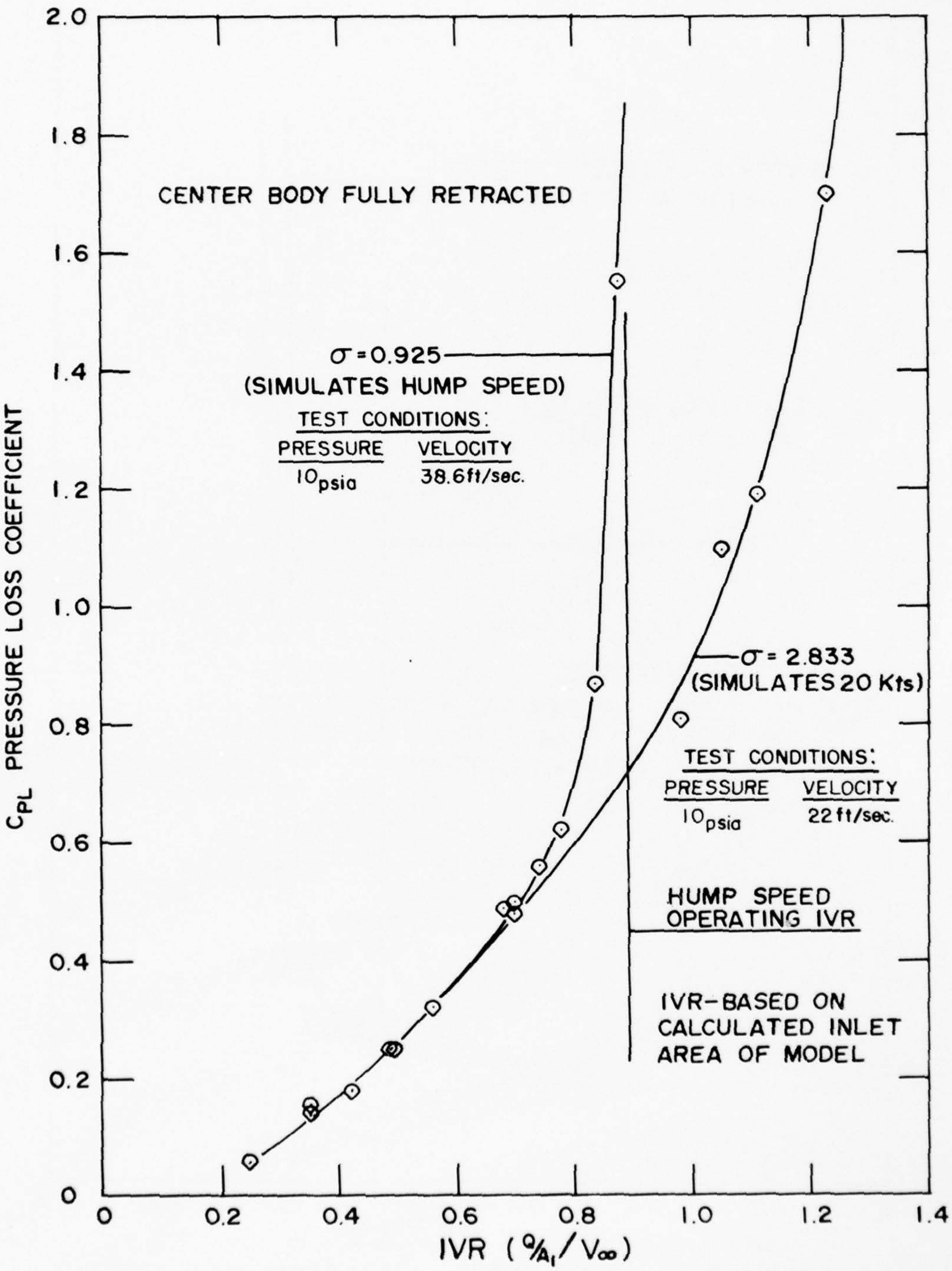

Figure 10. Internal Pressure Loss Performance—Low Speed Conditions.

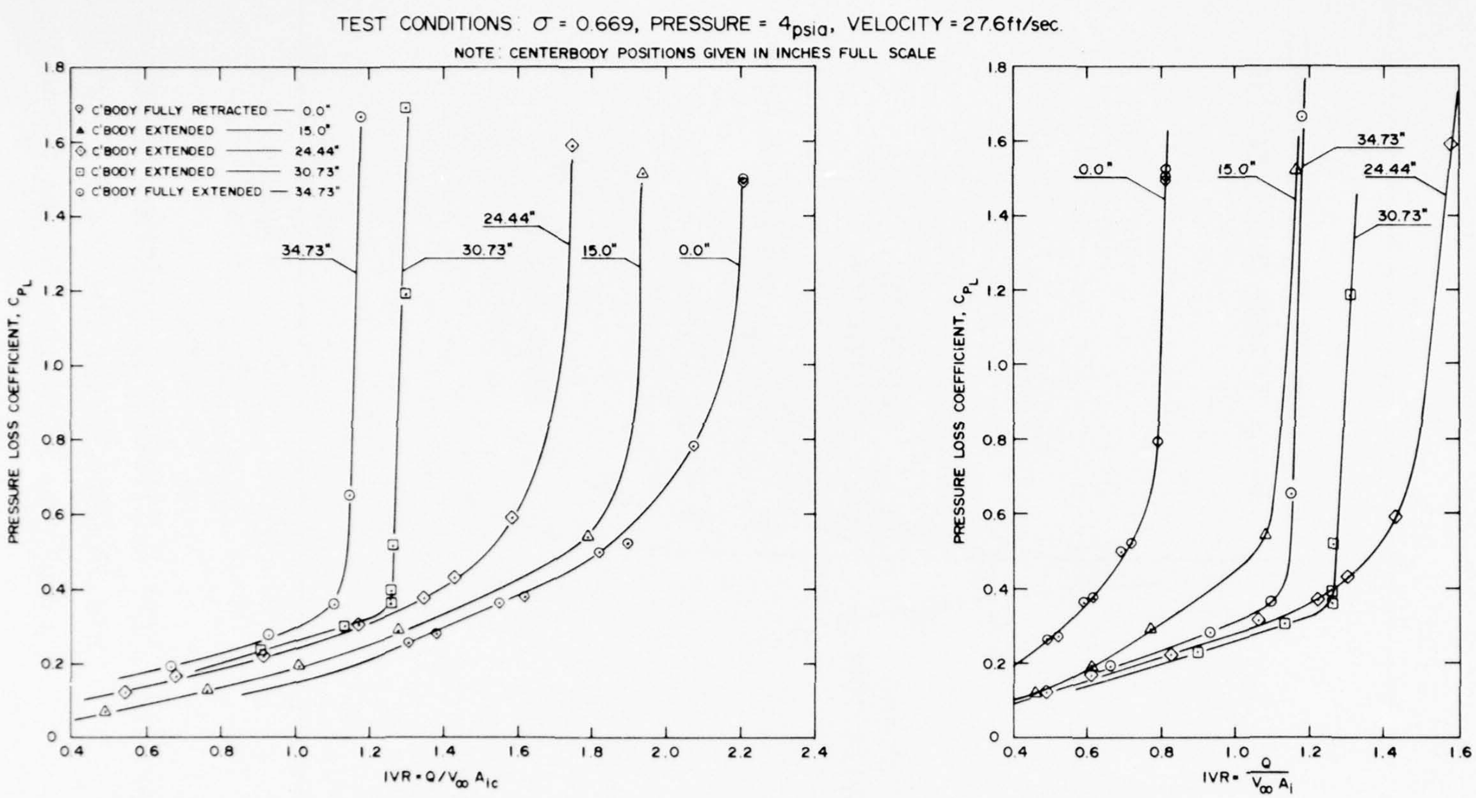

Figure 11. Comparison of Internal Pressure Loss Performance for Various Centerbody Positions.

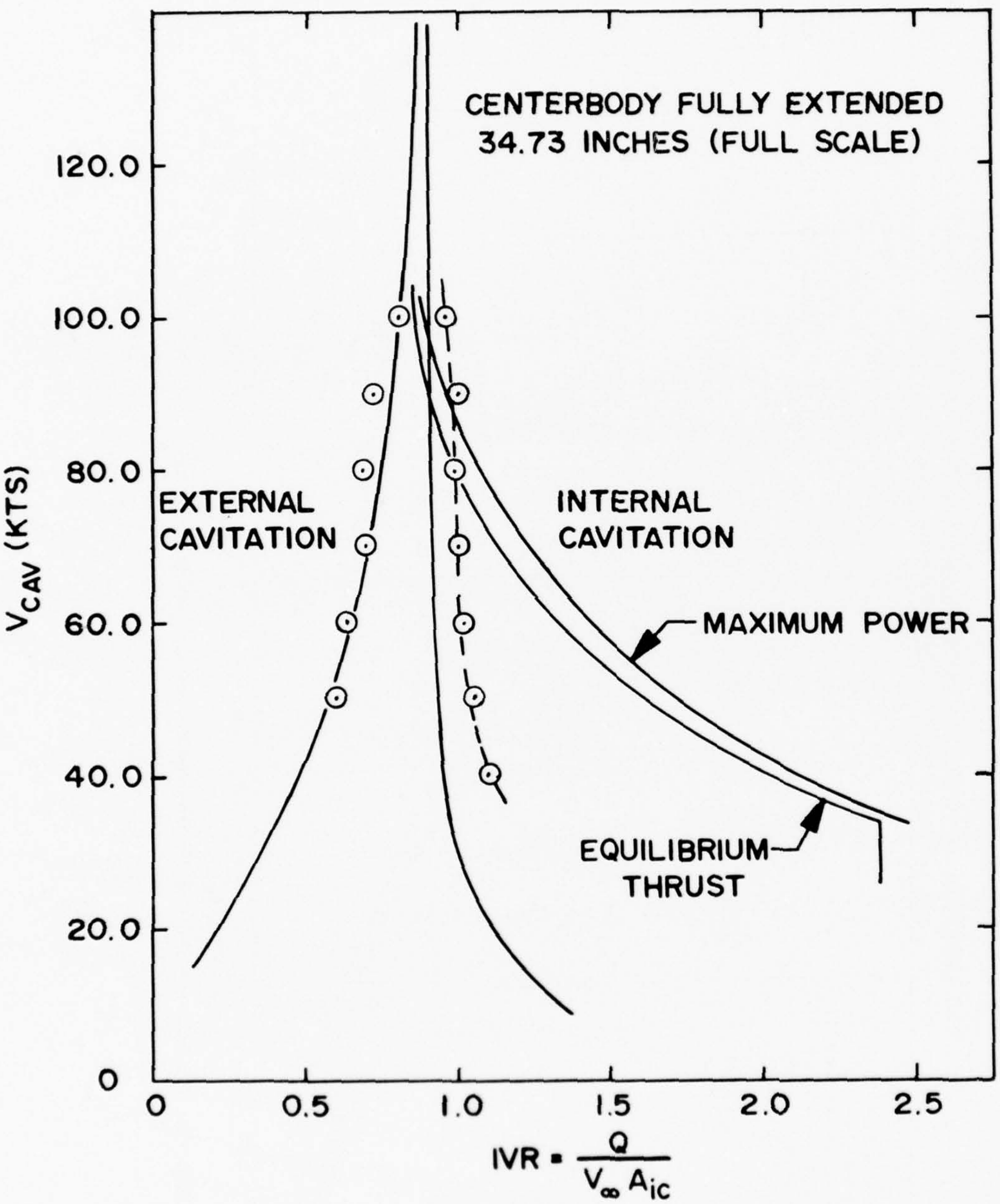

Figure 12–Inlet Cavitation Boundaries Measured and Predicted, for the 34.73 Inch (0.882m) Centerbody Extension (Fully Extended).

INTERNAL CAVITATION
σ=0.2275 (60 KNOTS)
IVR=1.036

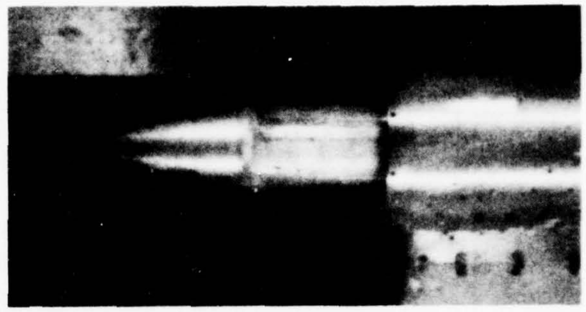

INTERNAL CAVITATION
σ=0.2275 (60 KNOTS)
IVR=1.052

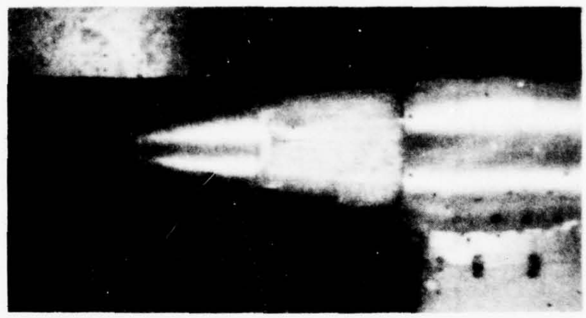

EXTERNAL CAVITATION
σ=0.1280 (80 KNOTS)
IVR=0.691

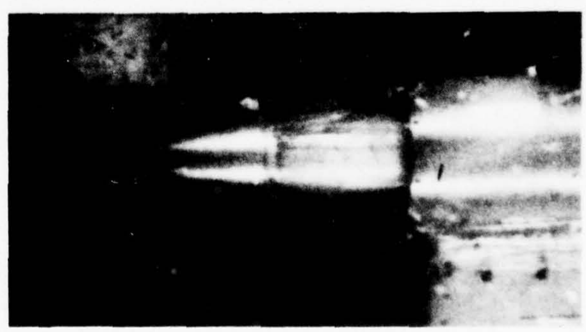

Figure 13—Photographs of Typical Inlet Cavitating Conditions for the 34.73 Inch (Full Scale) Centerbody Extension (Fully Extended)

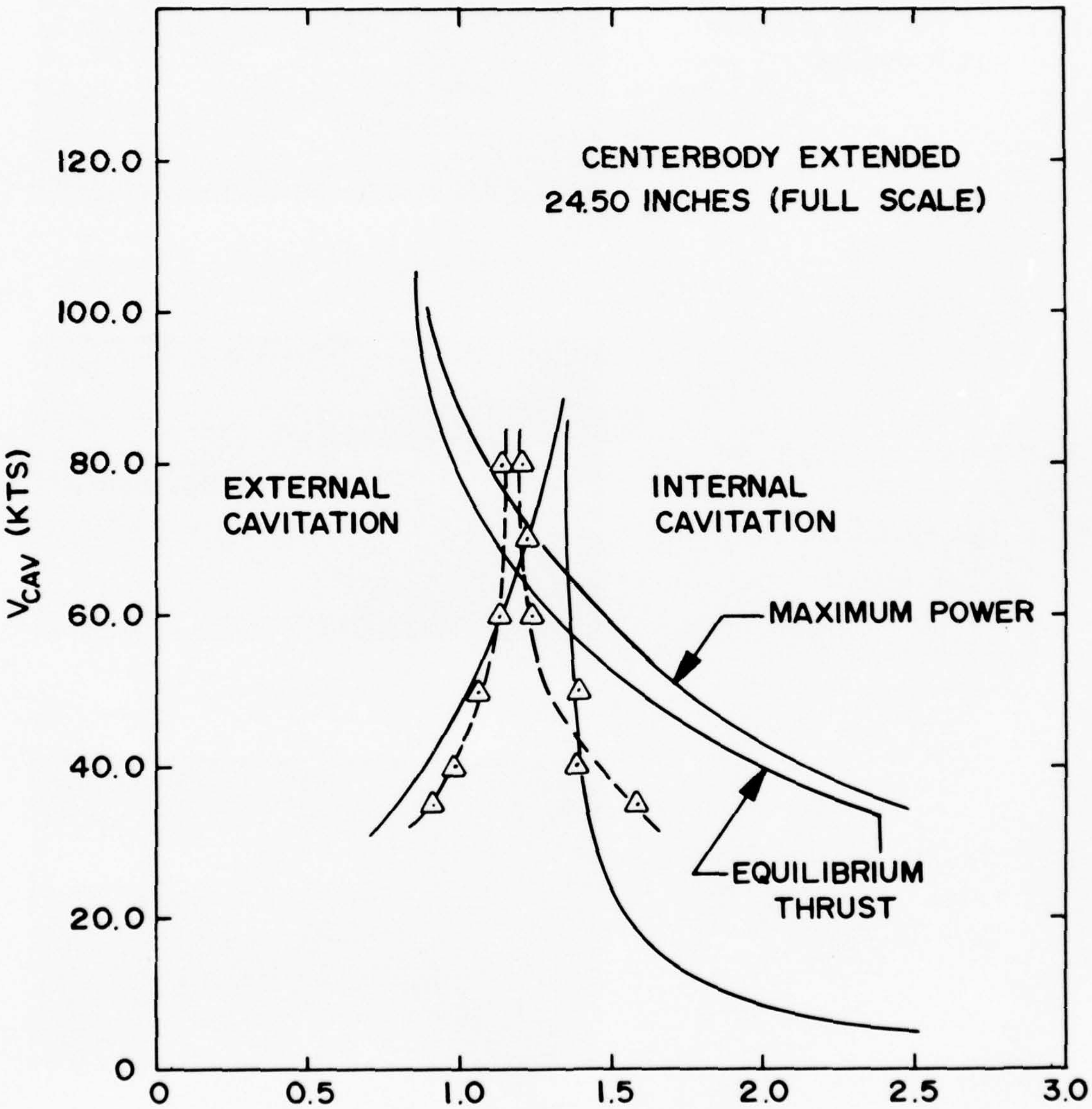

$$IVR = \frac{Q}{V_\infty A_{ic}}$$

Figure 14—Inlet Cavitation Boundaries Measured and Predicted, for the 24.44 Inch (0.621m) Centerbody Extension.

EXTERNAL CAVITATION
σ=0.2275 (60 KNOTS)
IVR = 1.08

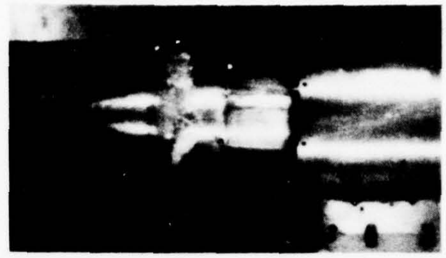

INTERNAL CAVITATION
σ=0.2275 (60 KNOTS)
IVR = 1.28

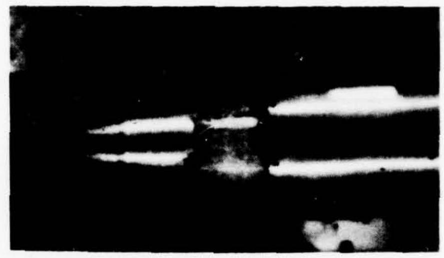

EXTERNAL CAVITATION
σ=0.5150 (40 KNOTS)
IVR = 0.65

INTERNAL CAVITATION
σ=0.5150 (40 KNOTS)
IVR = 1.59

Figure 15 - Photographs of Typical Inlet Cavitating Conditions for the 24.44 Inch (Full Scale) Centerbody Extension.

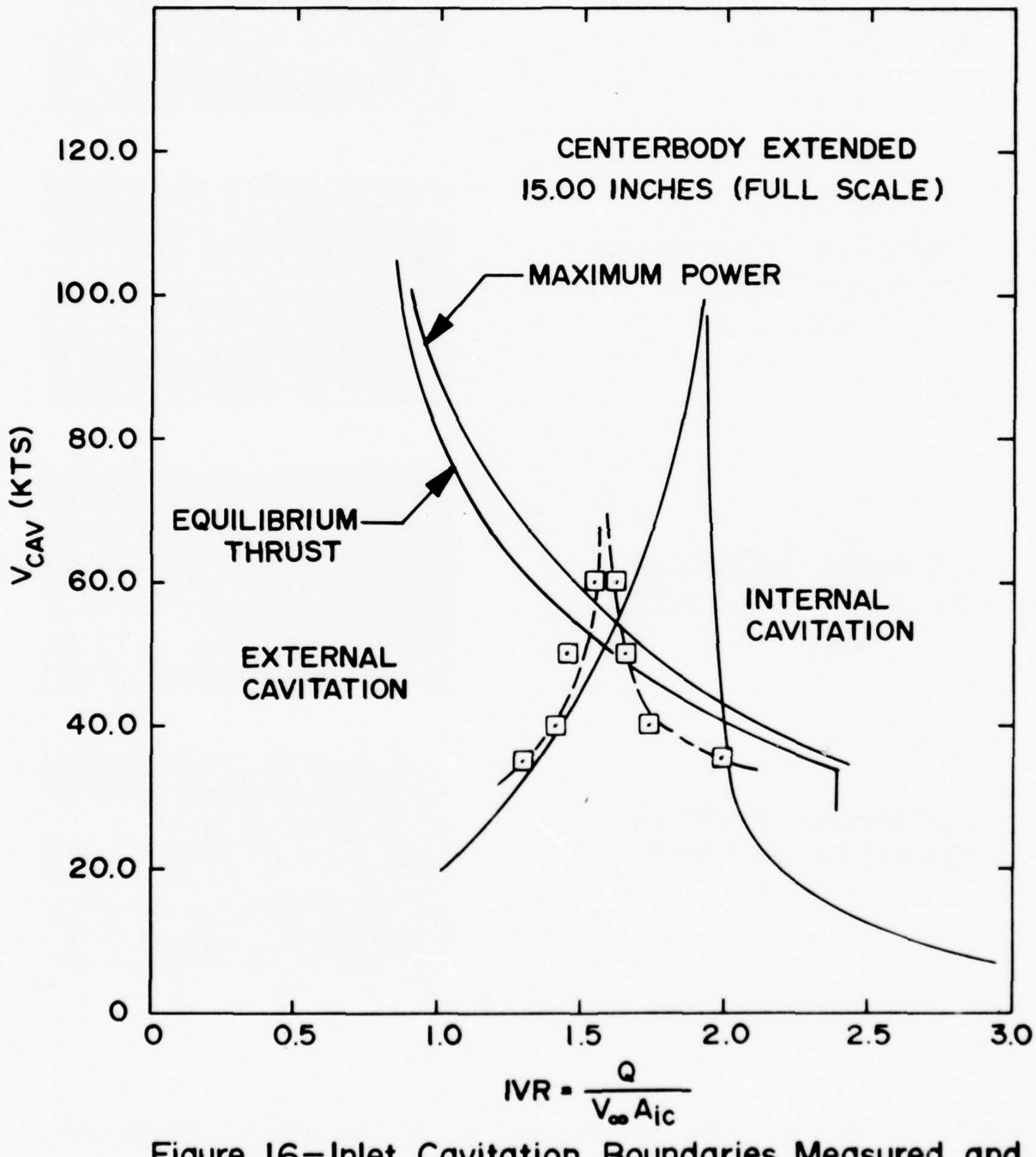

Figure 16—Inlet Cavitation Boundaries Measured and Predicted, for the 15.00 Inch (0.381m) Centerbody Extension.

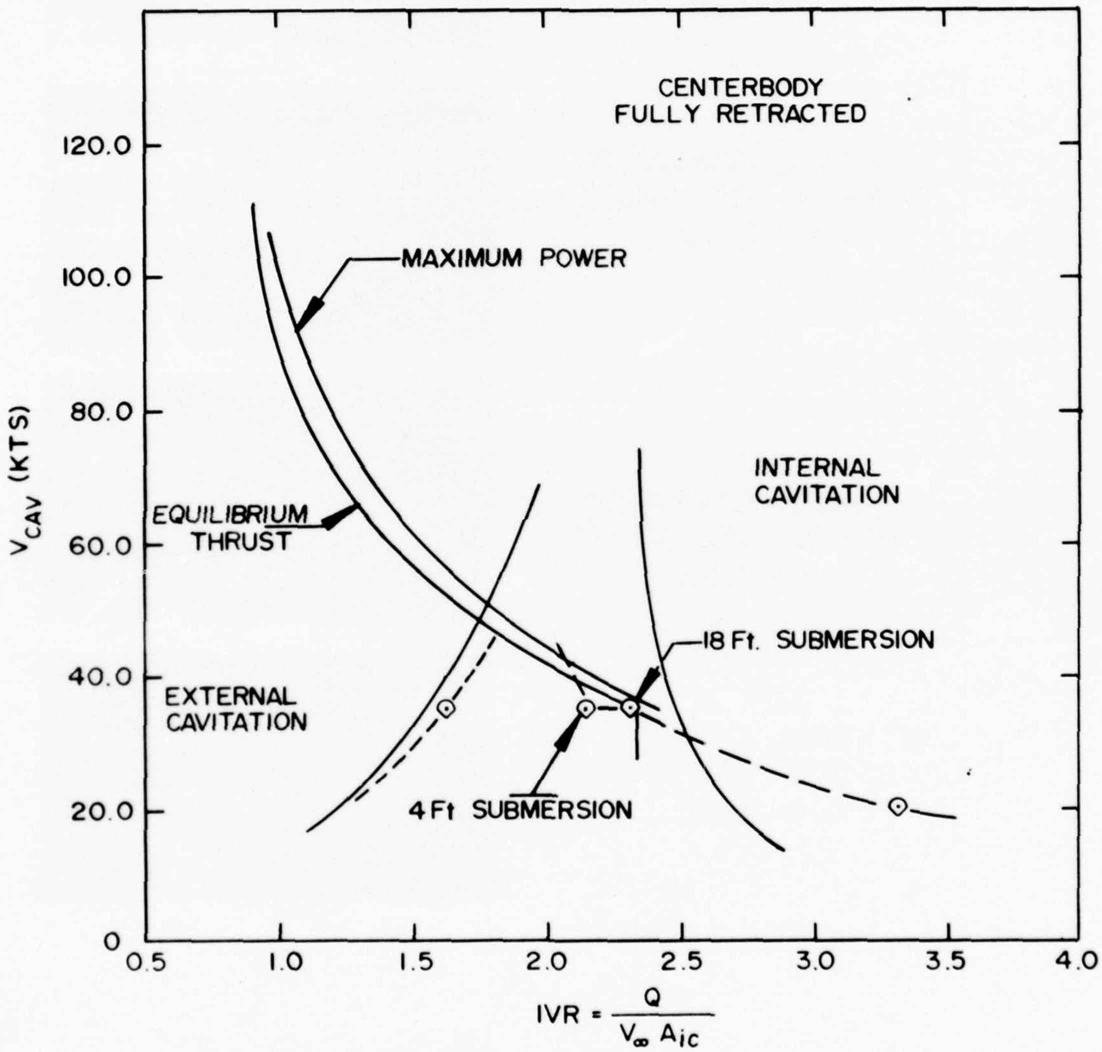

Figure 17–Inlet Cavitation Boundaries, Measured and Predicted, for the 0.0 Inch Centerbody Extension (Fully Retracted).

INTERNAL CAVITATION
σ=2.833 (20 KNOTS)
IVR = 3.32

INTERNAL CAVITATION
σ=2.833 (20 KNOTS)
IVR = 3.40

INTERNAL CAVITATION
σ=0.925 (35 KNOTS)
IVR = 2.33

INTERNAL CAVITATION
σ=0.925 (35 KNOTS)
IVR = 2.40

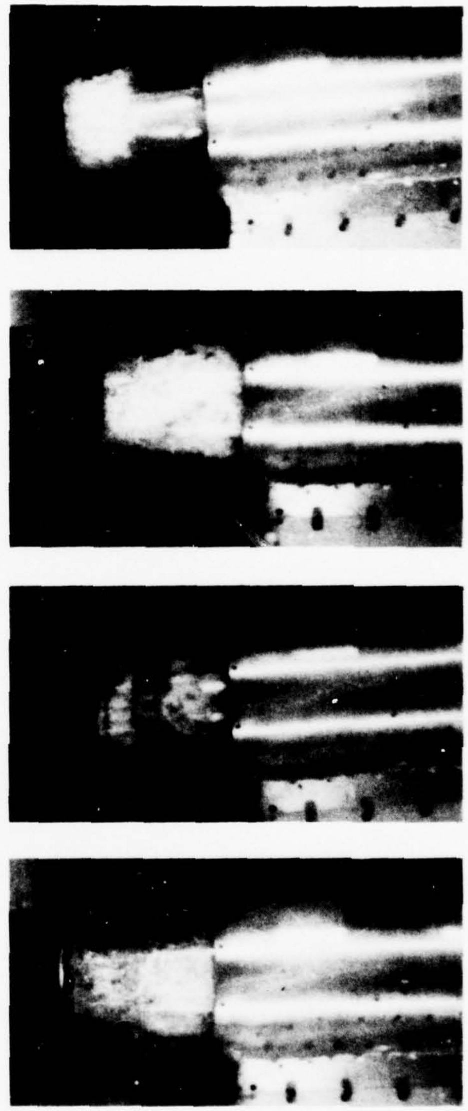

Figure 18—Photographs of Typical Inlet Cavitating Conditions for the 0.0 Inch (Full Scale) Centerbody Extension (Fully Retracted).

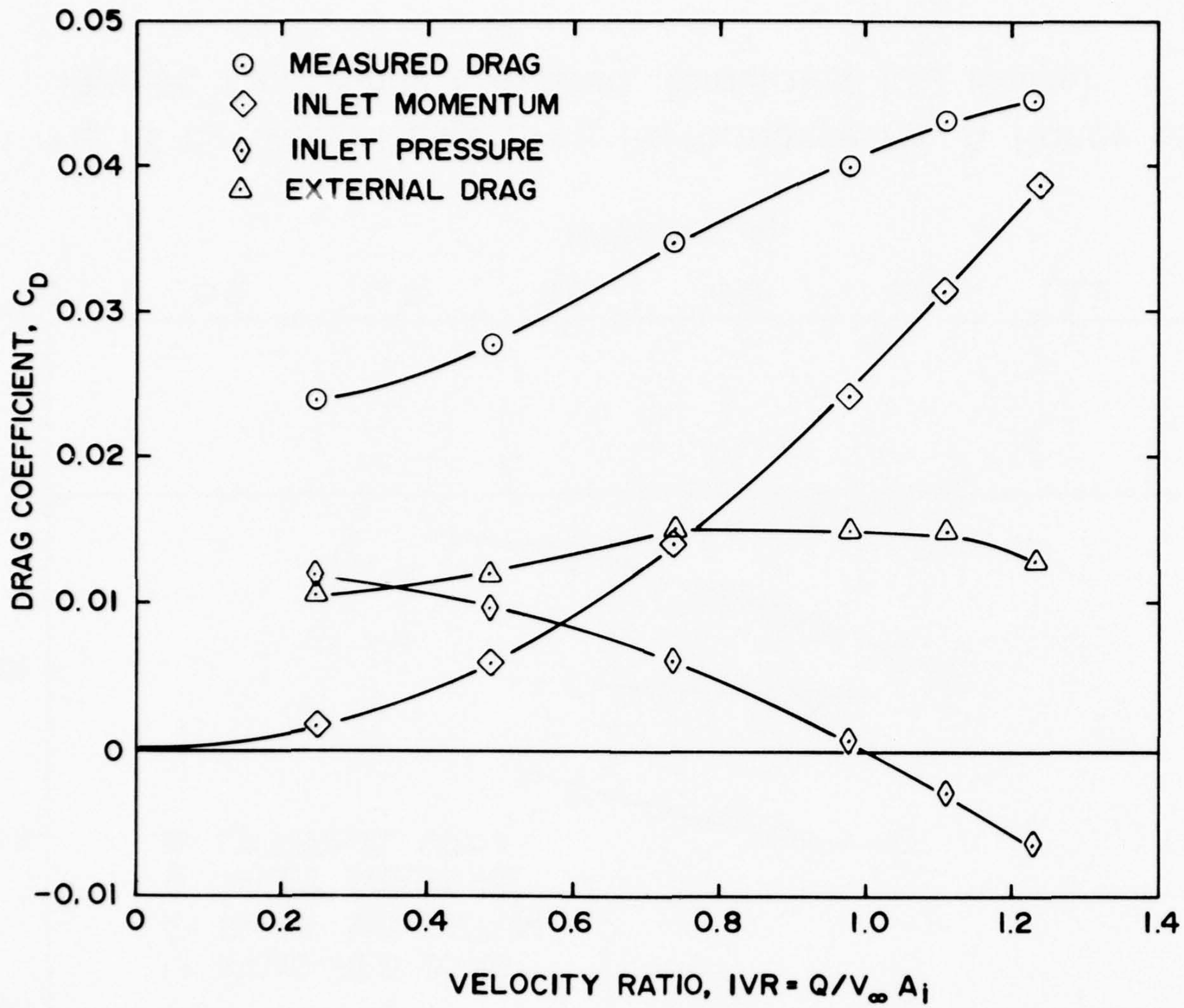

Figure 19–Typical Inlet Drag Performance for A Range of IVR (Plot-A, Centerbody Retracted, Simulated 20 Knots)

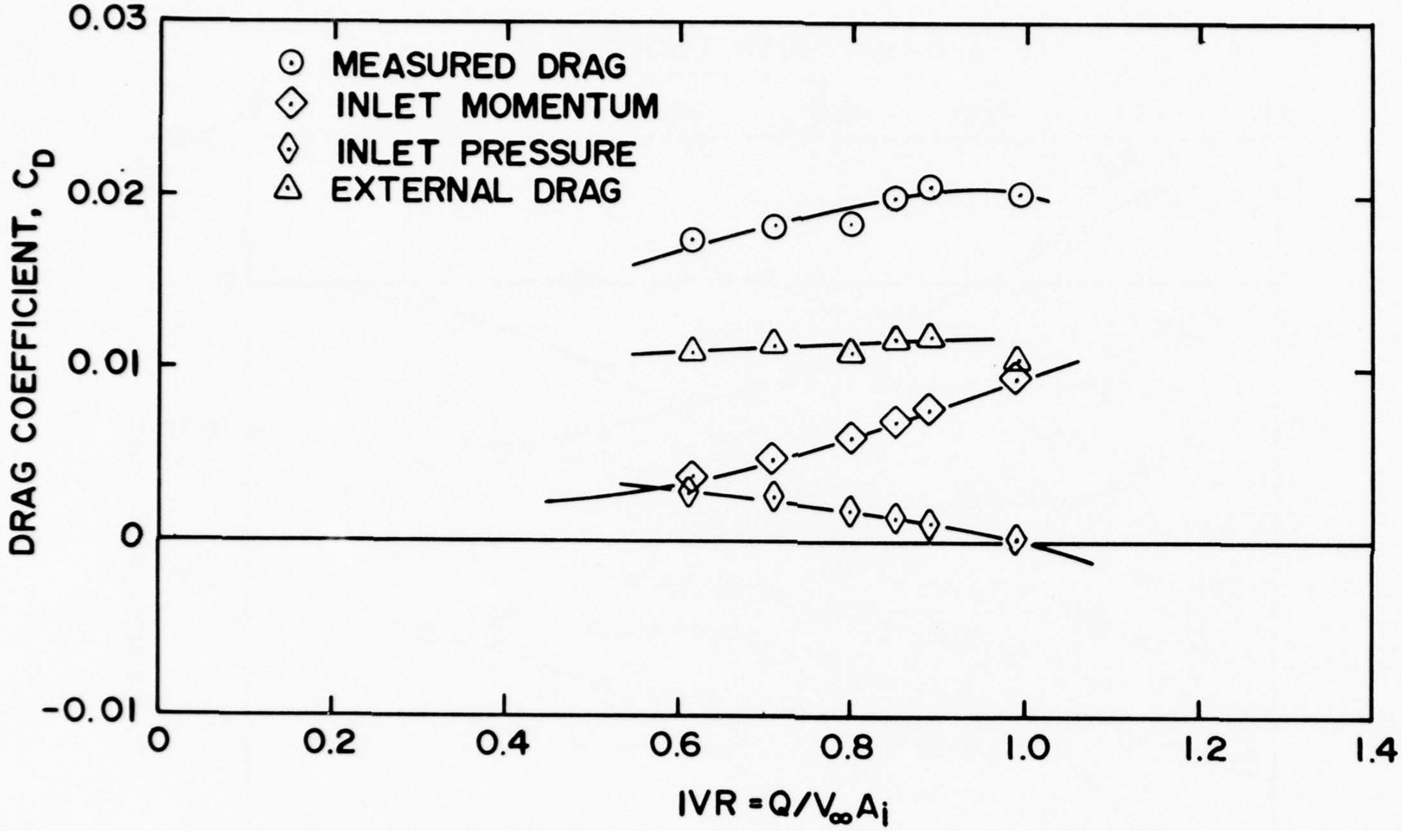

Figure 19—Typical Inlet Drag Performance for A Range of IVR (Plot-B, Centerbody Extended, Simulated 100 Knots)

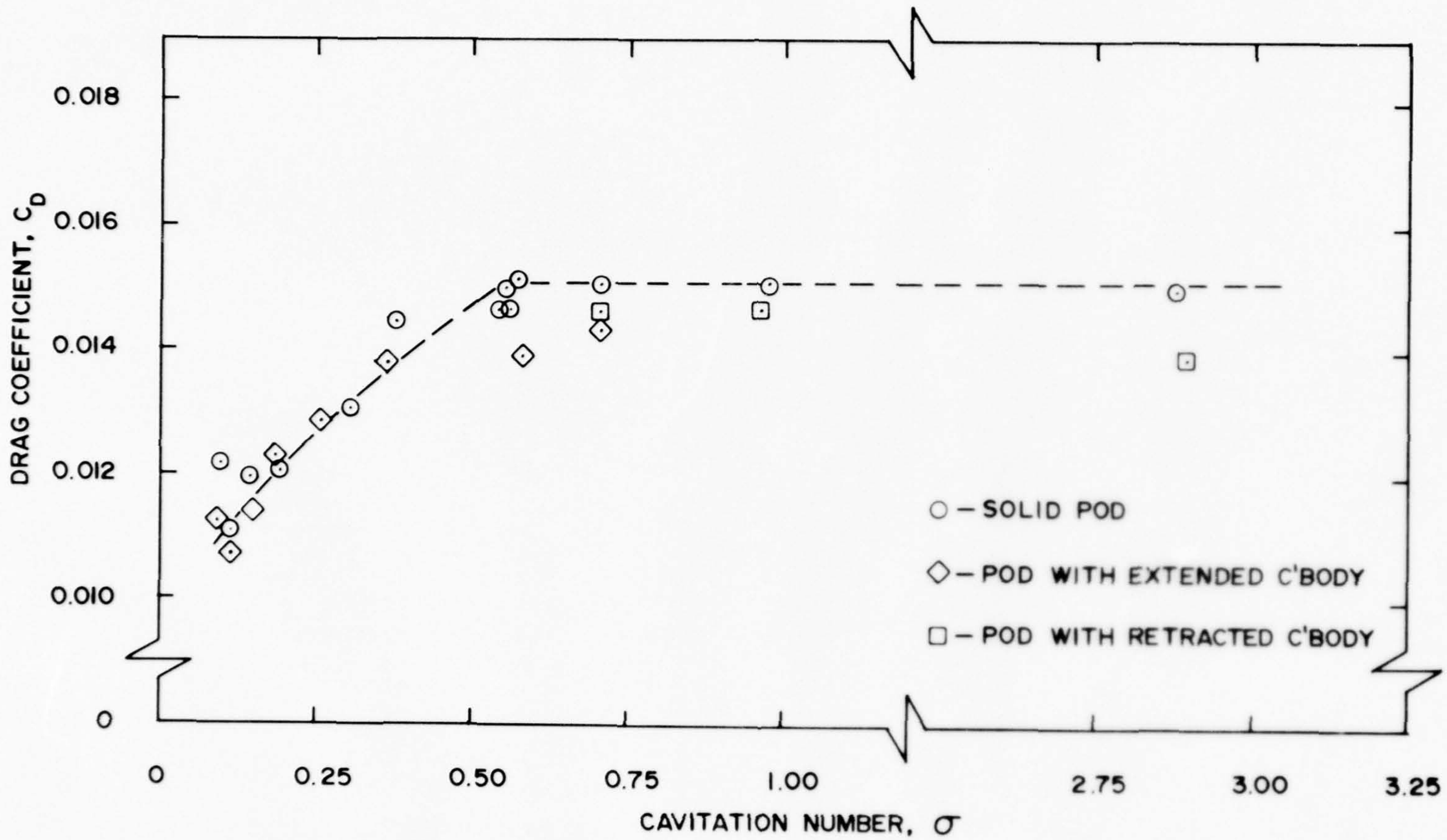

Figure 20–Pod–Strut Drag Performance

(Intentionally left blank)

APPENDIX A

PRELIMINARY POWERING REQUIREMENTS FOR THE PROPULSION SYSTEM OF A 200 TON, 100 KNOT HYDROFOIL SHIP

Hydrofoil Powering:

170 long tons

Take-off Speed = 35 knots
Cruise Speed = 100 knots

Thrust and Powering Required:

V (knots)	Thrust (lb)	Power (hp)
10	7,506	3,381
20	30,031	13,083
30,	67,617	29,070
35	91,981	39,701
40	85,959	37,315
50	76,929	34,184
60	70,258	32,427
70	64,983	31,591
80	60,830	31,561
90	57,349	32,200
100	54,400	33,509

Preliminary Pump Characteristics:

Cruise: V=100 Knots

head = 1100 ft
$\eta = 0.85$
$Q = 222\ ft^3/sec$*

Hump: V=35 Knots

head = 1265 ft
$\eta = 0.8$
$Q = 215.5\ ft^3/sec$

*Two Inlets

APPENDIX B

PROPOSED RESEARCH,
WORK STATEMENT,
LIST OF DELIVERABLES FOR CONTRACT NO. N00600-73-2-0964

"Design of a Pod Inlet for a 200 Ton, 100 Knot Hydrofoil"

PROPOSED RESEARCH (prepared by contractor)

Theoretical Design & Analysis

The previous section has pointed out some of the pitfalls and difficulties of high speed pod inlet design uncovered on the basis of a great deal of computer analysis performed at DSI on these systems. It is evident that considerable refinement of inlet shape is required to produce a workable design. Furthermore, there are a number of choices to make regarding inlet shape and type of inlet device used for high IVR operation. Pod slenderness must be weighed against internal flow diffusion requirements to minimize internal losses, and fluid mechanical efficiency of inlet devices must be considered in the light of mechanical complexity.

Thus, it is proposed to establish, based on DSI's past experience, a number of candidate pod and flush inlet designs to properly accomodate the IVR range and speed requirements of the 200 ton hydrofoil, subject to craft operating conditions supplied by the NSRDC Hydrofoil Program Office. These candidate inlets will be separated into the following three basic categories.

(1) Pod Inlet with Ring Slat

(2) Pod Inlet with Centerbody

(3) Flush Inlet with Seclected Inlet Device

Each of these inlets will be optimized to give their best performance, using the DSI axi-symmetric, two-dimensional and three-dimensional Neumann computer programs. Cruise optimization, of course, will be on the basis of achieving maximum ΔIVR centered on

the design IVR at V_{max} = 100 kts. Optimization at hump will involve the best shape and deployment position of the inlet device yielding ΔIVR = Max centered on the hump speed IVR.

The three optimized candidates will then be compared on the basis of cavitation boundaries, internal duct losses, external drag, and mechanical design considerations. On this basis, a judgement will be made as to the design which is the most suitable for application to the 200 ton hydrofoil design.

Once the best candidate has been selected, a detailed analysis of its performance through the entire IVR and inlet device deployment range will be made. In addition, the effect of inlet characteristics on the total waterjet propulsion system performance (as determined by using the above results in conjunction with the Pratt & Whitney Mapping Program, currently computer-operational at DSI) will be assessed throughout the craft's operating regime.

REFERENCES

1) Pratt & Whitney Aircraft — Waterjet Performance Mapping Computer Program Final Technical Report, PWAFR-3434-3442 January 23, 1970

2) Aerojet General Corporation — Fifth Scale Pod-Auxiliary Test Program, SES-E-E003-16 February 1971

STATEMENT OF WORK (prepared by contractor)

Meeting with contract monitor to obtain relevant craft information needed for inlet design. This will include operating speed and pump mass flow envelope, craft drag characteristics, configuration constraints and sizes, etc.

Design, using quasi-two-dimensional methods of three basic inlets suitable for the craft under consideration, satisfying the hydromechanical and configurational requirements. These will include:

a) Ring slat pod

b) Centerbody pod

c) Flush inlet

Analyze the basic pod or flush inlet hydrodynamics using the axisymmetric or 2-D Newmann programs respectively for maximum speed IVR (lip device undeployed). For this purpose, at least three variations on each basic configuration will be designed and analyzed. The best of each basic configuration will be selected.

Analyze each of the selected inlets with the lip devices deployed for:

a) Static thrust

b) Hump speed

Analyze the external flow about the pod/strut combination for high speed operation.

Select the best overall inlet for final refinement and analysis over entire IVR operating range.

Using Pratt & Whitney waterjet mapping program (reference (1)) determine overall inlet/pump/nozzle performance in terms of thrust/power, yielding vehicle acceleration, margin over hump, max-speed, cavitation damage, etc.

PROGRAM SCHEDULE AND ORGANIZATION (prepared by contractor)

Schedule

The Aerospace Technology Division of Developmental Sciences, Inc., proposes to perform the tasks outlined in section 3 within a 6 month period. The detailed schedule for the various tasks and milestones are shown in the figure of the Project Schedule.

Program Organization

Developmental Sciences , Inc., proposes to perform the tasks outlined within the specified period. DSI-AT is equipped to undertake the proposed program, not only in terms of technical and management skills, but also in terms of organization, facilities and financial capability.

The organization for this project is shown in the Figure. Dr. Gordon L. Harris will act as technical program manager for the proposed program. Dr. Michel El Raheb will serve as the project scientist. Dr. Harris reports to Dr. Gerald R. Seemann, President

of DSI. All of these men are very competent engineers and scientists with experience that is pertinent and relevant to the proposed program.

A brief outline of the project duties for each lead man and the time he is expected to devote to the project is specified.

1. Dr. G. L. Harris (15% time) - will lead the design and analysis and serve as overall technical coordinator.

2. Dr. M. El Raheb (50% time) - will participate in the Newmann analysis of the inlet, pod/strut analysis, model scaling and data interpretation phases of the project.

3. Dr. G. R. Seemann - will at no charge to the program insure that the corporation meets its technical, financial, and schedule obligations as set forth herein.

PROJECT SCHEDULE

MONTHS

TASKS

1. Meeting with monitor
2. Design of three basic configurations
3. High speed configuration Neumann analysis
4. Zero and hump speed analysis
5. Pod/strut interaction analysis
6. Selection of best scheme and complete IVR analysis
7. Waterjet mapping analysis

   Briefing and Interchange

8. Final report preparation (draft)

   Final Report (after NSRDC Review)

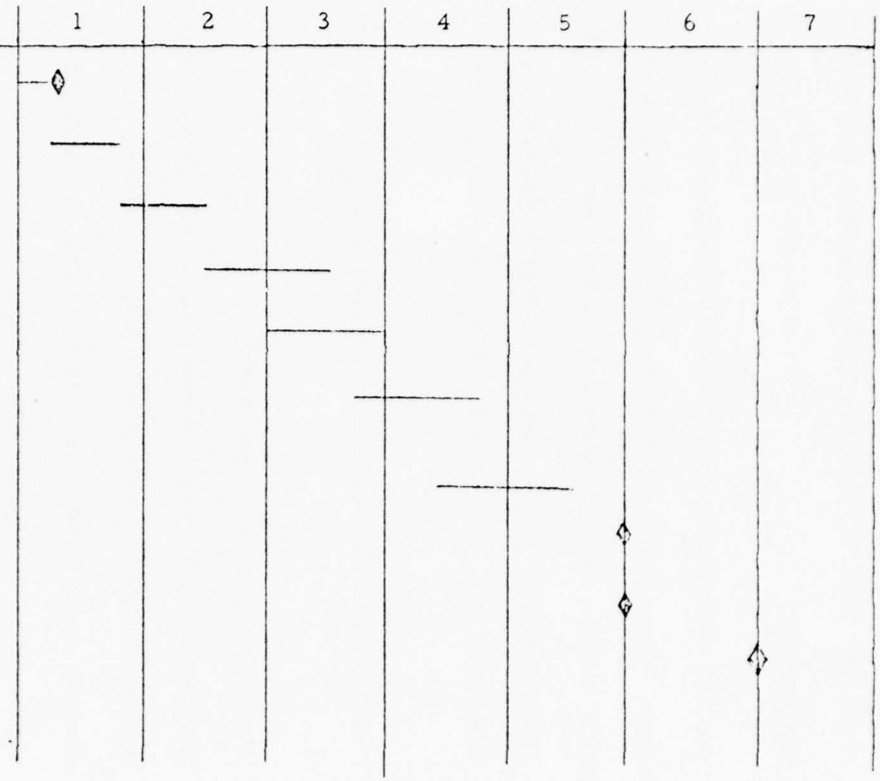

WORK STATEMENT AND DELIVERABLE ITEMS (prepared by DTNSRDC)

Work Statement

The DSI will design and deliver preliminary design drawings for a Waterjet Inlet-Pod-Strut system to be used on a 200-ton, 100-knot hydrofoil craft. Two of these inlets will be used on the (2) aft foil systems of the craft, having a canard configuration (single foil fwd, two foils aft, with a 35% - 65% load distribution).

NSRDC (Code 1532) will provide the following information:

Available power vs speed curve

Minimum speed at which maximum power should be utilized

Maximum allowable velocity to the pump-inlet

Drag vs craft speed, exclusive of the two strut-pod

Approximate strut-wing dimension

DSI will conduct:

A screening analysis of a number of strut-pod-inlet configurations accomodating the IVR range and speed for the craft's operating envelop.

Select (3) arrangements for detailed comparison of head-recovery, duct losses, external drag and cavitation inception boundaries. Select the "best" arrangement providing cavitation-degradation-free performance over the craft's operational envelop, based on the least amount of head-loss, the least external drag, cavitation-degradation

sensitivity to pitch and yaw, and mechanical complexity. This selection will be finalized after approval has been obtained from Code 1532,NSRDC.

Final, detailed analysis of the selected inlet-pod-strut configuration.

Preliminary design drawings of the configuration.

Deliver a final report describing in detail, the work performed including the method used and presenting the detailed calculations for each phase of the work statement.

The design drawings of the final configuration will be included in the report, as well as the predicted performance of the strut-pod-inlet system throughout the craft's speed range, inclusive of the performance over the IVR range and inlet device deployment range, showing the cavitation inception boundaries, internal duct losses, external drag, and mechanical deployment modes.

Conclusions and recommendations will also be made.

Time Schedule

The contract is let for 6 months duration, a rough draft of the final report to be submitted within six months after the inception of the program. This draft will be reviewed by Code 1532, NSRDC, and the final report issued reflecting the modifications suggested after review.

Monthly letter reports, describing "progress to date", will be delivered by DSI to Code 1532, NSRDC. The letter report will state:

Accumulated expenditures

Accomplishments to-date

Problems encountered

Solutions proposed

Predicted progress for next period

APPENDIX C

MODEL DATA - TABLE OF OFFSETS

BASIC DIMENSIONS OF THE MODEL

POD:

Length from leading edge of inlet lip to tail (faired boatail configuration)........................29.0 inch (0.7366 m)

Length from leading edge of inlet lip to blunt base (blunt base configuration)......................22.77 inch (0.5784 m)

Length from leading edge of centerbody to tail (boatail, fully extended centerbody).................34.4 inch (0.8738 m)

Maximum external diameter.............................5.445 inch (0.1383 m)

Diameter at blunt base................................4.02 inch (0.1021 m)

Base area...12.69 $inch^2$ ($8.187 \times 10^{-3} m^2$)

Estimate of wetted area (blunt base).................372 $inch^2$ ($0.240\ m^2$)

STRUT: Parabolic shape, nominal t/c = 12%

Length at pod intersection............................16.5 inch (0.4191 m)

Length at 17 inch (0.4318 m) from pod intersection....18.5 inch (0.4699 m)

Length at mating flange...............................20.25 inch (0.5144 m)

Assumed height for strut wetted area.................17 inch (0.4318 m)

Assumed height for strut base area...................17 inch (0.4318 m)

Thickness at strut base...............................2.24 inch (0.0569 m)

Estimate of wetted area...............................560 $inch^2$ (0.3613 m)

Estimate of base area.................................38.08 $inch^2$ (0.02457 m)

INLET AREA SCHEDULE

Position	Centerbody Extension Full Scale	Inlet Area Full Scale	Inlet Area Model
1	34.73 inch (0.882 m)	0.7740 ft^2 (0.0719 m^2)	0.03096 ft^2 ($1.997 \times 10^{-5} m^2$)
2	30.73 inch (0.7805 m)	0.7743 ft^2 (0.07193 m^2)	0.03097 ft^2 ($1.998 \times 10^{-5} m^2$)
3	24.44 inch (0.6208 m)	0.8578 ft^2 (0.0797 m^2)	0.03431 ft^2 ($2.214 \times 10^{-5} m^2$)
4	15.00 inch (0.381 m)	1.2848 ft^2 (0.1194 m^2)	0.05139 ft^2 ($3.315 \times 10^{-5} m^2$)
5	0.00 inch (0.0 m)	2.0443 ft^2 (0.1899 m^2)	0.08177 ft^2 ($5.275 \times 10^{-5} m^2$)

BODY NUMBER 1 (CENTERBODY)

NO	X	Y	NO	X	Y	NO	X	Y
1	0.00000	0.00000	34	4.16627	3.73196	67	30.80399	7.62973
2	.00186	.08060	35	4.48905	3.86688	68	32.37866	7.62973
3	.00779	.16492	36	4.82939	4.00313	69	34.00615	7.62973
4	.01831	.25286	37	5.18814	4.14071	70	35.68824	7.62973
5	.03394	.34426	38	5.56614	4.27962	71	37.42674	7.62973
6	.05519	.43892	39	5.96431	4.41984	72	39.22355	7.62973
7	.08250	.53657	40	6.38361	4.56135	73	41.08063	7.62973
8	.11629	.63694	41	6.82504	4.70409	74	43.00000	7.62973
9	.15692	.73976	42	7.28966	4.84801	75	44.95091	7.62973
10	.20472	.84474	43	7.77859	4.99306	76	46.90182	7.62973
11	.25996	.95164	44	8.29301	5.13913	77	48.85272	7.62973
12	.32287	1.06023	45	8.83413	5.28613	78	50.80363	7.62973
13	.39367	1.17030	46	9.40327	5.43392	79	52.75454	7.62973
14	.47256	1.28168	47	10.00178	5.58235	80	54.70545	7.62973
15	.55972	1.39427	48	10.63110	5.73125	81	56.65635	7.62973
16	.65536	1.50796	49	11.29272	5.88038	82	58.60726	7.62973
17	.75966	1.62267	50	11.98823	6.02948	83	60.55817	7.62973
18	.87286	1.73836	51	12.71930	6.17824	84	62.50908	7.62973
19	.99518	1.85502	52	13.48766	6.32628	85	64.45999	7.62973
20	1.12689	1.97264	53	14.29516	6.47316	86	66.41089	7.62973
21	1.26827	2.09120	54	15.14372	6.61832	87	68.36180	7.62973
22	1.41962	2.21073	55	16.03536	6.76113	88	70.31271	7.62973
23	1.58128	2.33126	56	16.97221	6.90074	89	72.21613	7.62973
24	1.75362	2.45282	57	17.95652	7.03615	90	74.03859	7.62973
25	1.93703	2.57542	58	18.99063	7.16605	91	75.78352	7.62973
26	2.13194	2.69913	59	20.07702	7.28875	92	77.45424	7.62973
27	2.33878	2.82395	60	21.21830	7.40188	93	79.05389	7.62973
28	2.55807	2.94994	61	22.41721	7.50198	94	80.58550	7.62973
29	2.79030	3.07711	62	23.67664	7.58313	95	82.05196	7.62973
30	3.03604	3.20552	63	25.00000	7.62973	96	83.45604	7.62973
31	3.29586	3.33519	64	26.38000	7.62973	97	84.80040	7.62973
32	3.57040	3.46613	65	27.80629	7.62973	98	86.08757	7.62973
33	3.86030	3.59838	66	29.28041	7.62973	99	87.32000	7.62973

BODY NUMBER 2

NO	X	Y	NO	X	Y	NO	X	Y
1	49.11934	12.23720	34	10.69609	10.18282	67	1.80622	9.71703
2	47.04771	12.23720	35	10.18238	10.10216	68	1.69754	9.72053
3	45.06705	12.23720	36	9.69154	10.03178	69	1.59406	9.72409
4	43.17336	12.23720	37	9.22267	9.97061	70	1.49555	9.72768
5	41.36280	12.23720	38	8.77490	9.91768	71	1.40176	9.73131
6	39.63176	12.23720	39	8.34738	9.87213	72	1.31248	9.73496
7	37.97674	12.23720	40	7.93924	9.83319	73	1.22747	9.73863
8	36.39437	12.23720	41	7.54970	9.80013	74	1.14656	9.74231
9	34.86833	12.23043	42	7.17794	9.77233	75	1.06952	9.74602
10	33.34267	12.19555	43	6.82322	9.74919	76	.99619	9.74972
11	31.84905	12.13889	44	6.48478	9.73020	77	.92637	9.75344
12	30.41897	12.08139	45	6.16189	9.71489	78	.85991	9.75717
13	29.04974	12.02296	46	5.85391	9.70284	79	.79665	9.76091
14	27.73878	11.96347	47	5.56013	9.69366	80	.73643	9.76466
15	26.48365	11.90282	48	5.27995	9.68702	81	.67911	9.76842
16	25.28201	11.84085	49	5.01274	9.68259	82	.62454	9.77218
17	24.13158	11.77741	50	4.75790	9.68011	83	.57260	9.77596
18	23.03025	11.71230	51	4.51489	9.67933	84	.52316	9.77977
19	21.97595	11.64528	52	4.27637	9.67958	85	.47611	9.78359
20	20.96674	11.57613	53	4.04928	9.68033	86	.43133	9.78743
21	20.00075	11.50449	54	3.83307	9.68148	87	.38872	9.79132
22	19.07623	11.42998	55	3.62722	9.68301	88	.34817	9.79525
23	18.19151	11.35214	56	3.43122	9.68484	89	.30959	9.79924
24	17.34502	11.27039	57	3.24463	9.68694	90	.27288	9.80330
25	16.53529	11.18396	58	3.06698	9.68928	91	.23795	9.80745
26	15.76097	11.09191	59	2.89784	9.69183	92	.20476	9.81171
27	15.02090	10.99295	60	2.73681	9.69456	93	.17319	9.81613
28	14.31406	10.88535	61	2.58350	9.69745	94	.14319	9.82074
29	13.63982	10.76664	62	2.43754	9.70047	95	.11471	9.82561
30	12.99799	10.63320	63	2.29858	9.70360	96	.08771	9.83085
31	12.38363	10.49860	64	2.16627	9.70684	97	.06216	9.83664
32	11.79580	10.37967	65	2.04031	9.71017	98	.03815	9.84336
33	11.23360	10.27489	66	1.92039	9.71357	99	.01599	9.85191

BODY NUMBER 2 (POD)

NO	X	Y	NO	X	Y	NO	X	Y
100	0.00000	9.86788	133	1.53042	10.63461	166	10.05210	12.12858
101	.00088	9.89046	134	1.63649	10.66216	167	10.58557	12.20393
102	.00526	9.91377	135	1.74795	10.69032	168	11.14584	12.28131
103	.01278	9.93748	136	1.86505	10.71910	169	11.73426	12.36067
104	.02343	9.96131	137	1.98808	10.74856	170	12.35224	12.44189
105	.03712	9.98501	138	2.11732	10.77870	171	13.00129	12.52486
106	.05368	10.00846	139	2.25305	10.80957	172	13.68297	12.60944
107	.07295	10.03161	140	2.39560	10.84122	173	14.39892	12.69544
108	.09479	10.05444	141	2.54531	10.87366	174	15.15089	12.78265
109	.11911	10.07697	142	2.70251	10.90693	175	15.94067	12.87081
110	.14580	10.09925	143	2.86756	10.94110	176	16.77018	12.95964
111	.17485	10.12130	144	3.04086	10.97617	177	17.64140	13.04876
112	.20623	10.14319	145	3.22281	11.01222	178	18.55646	13.13778
113	.23993	10.16497	146	3.41381	11.04927	179	19.51756	13.22622
114	.27601	10.18667	147	3.61433	11.08739	180	20.52698	13.31355
115	.31448	10.20836	148	3.82481	11.12661	181	21.58716	13.39914
116	.35541	10.23006	149	4.04574	11.16698	182	22.70065	13.48227
117	.39886	10.25183	150	4.27764	11.20856	183	23.87010	13.56216
118	.44490	10.27370	151	4.52104	11.25141	184	25.09829	13.63785
119	.49365	10.29570	152	4.77716	11.29592	185	26.38816	13.70832
120	.54518	10.31786	153	5.04610	11.34224	186	27.74274	13.77240
121	.59960	10.34022	154	5.32851	11.39043	187	29.16523	13.82872
122	.65705	10.36281	155	5.62506	11.44055	188	30.65897	13.87580
123	.71764	10.38567	156	5.93645	11.49262	189	32.22743	13.91194
124	.78150	10.40880	157	6.26345	11.54670	190	33.87424	13.93524
125	.84878	10.43225	158	6.60683	11.60283	191	35.60319	13.94355
126	.91964	10.45605	159	6.96742	11.66105	192	37.29858	13.94355
127	.99422	10.48022	160	7.34609	11.72137	193	38.99397	13.94355
128	1.07272	10.50479	161	7.74375	11.78384	194	40.68936	13.94355
129	1.15530	10.52980	162	8.16135	11.84847	195	42.38475	13.94355
130	1.24214	10.55524	163	8.59990	11.91526	196	44.08014	13.94355
131	1.33347	10.58118	164	9.06046	11.98421	197	45.77553	13.94355
132	1.42949	10.60763	165	9.54414	12.05533	198	47.47092	13.94355

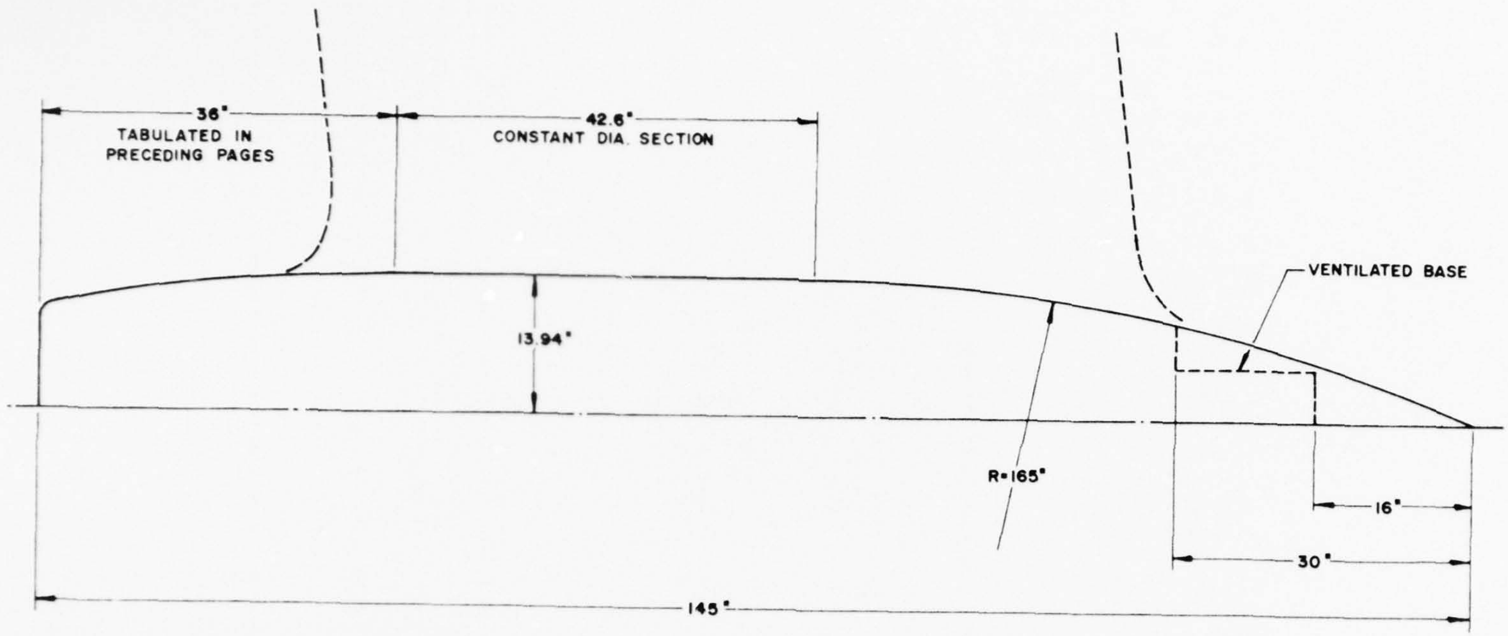

EXTERNAL POD SHAPE

(Intentionally left blank)

APPENDIX D

LISTING OF DATA REDUCTION PROGRAM USED FOR THE ANALYSIS OF PRESSURE DATA

```
CHASWJP,CM50000,P3.                                             1532.SOBOLEWSKI
CHARGE,CHAS,1272116502,CC,J.
FTN(T,A)
LGO.
EXIT.
  0000000000000000000
        PROGRAM  WJETD(INPUT,OUTPUT,TAPE5=INPUT,TAPE6=OUTPUT)
C AL SOBOLEWSKI     CODE 1532    X71318
        DIMENSION GPM(21),DRAG(21),VFS(21),PT(21),P(36,21),Q(21),
       1PODEX(8), CPF(13,21),CPI(35,21),PAVG1(21),PAVG2(21),PAVG3(21),
       2          PAVG4(21),PAVG5(21),PAVG6(21),VIN(21),AREA(21)
        DIMENSION CPL(21),CPLT(21),SIGMA(21),RE(21),PTOT(21),PLOC(21),
       1 IVRA(21), IVRB(21), CPLF(21), CPLTF(21)
        INTEGER RUN(21),PODEX(8)
        REAL LIFT(21),KV,IVRA, IVRB, CPLF, CPLTF
        READ (5,721) RHO
        READ (5,721) PV
        READ (5,735) KV
        READ (5,701) NSETS
        DO 300 J=1,NSETS
        WRITE (6,717) J
        READ (5,719) ASIGMA,APODEX,AFSS
C    ASSIGN INLET AREA
        READ (5,715) PODEX(K)
        IF (PODEX(K)-412) 931,932,933
  931 AREAA=0.03097
        D=0.069
        GO TO 935
  932 AREAA=0.03431
        D=0.0775
        GO TO 935
  933 IF (PODEX(K)-1057) 936,937,938
  936 AREAA=0.05139
        D=0.1267
        GO TO 935
  937 AREAA=0.06781
        GO TO 935
  938 AREAA=0.08177
        D=0.3233
  935 CONTINUE
        READ (5,701) NRUNS
C    READ DATA
        DO 400 IY=1,NRUNS
        READ (5,718) RUN(IY),GPM(IY),DRAG(IY),LIFT(IY),VFS(IY),PT(IY)
        READ (5,704)(P(IX,IY),IX=1,35)
        Q(IY)=GPM(IY)*0.002228
        VIN(IY)=Q(IY)/AREAA
        IVRA(IY) = VIN(IY) / VFS(IY)
        IVRB(IY) = (Q(IY)/0.03097) / VFS(IY)
        DO 350 IX=1,4
        CPF(IX,IY)=((P(IX,IY)-PT(IY))*144.)/(.5*RHO*VFS(IY)**2.)
  350 CONTINUE
        DO 450 IX=9,13
        CPF(IX,IY)=((P(IX,IY)-PT(IY))*144.)/(.5*RHO*VFS(IY)**2.)
  450 CONTINUE
        DO 550 IX=17,35
        CPI(IX,IY)=((P(IX,IY)-PT(IY))*144.)/(.5*RHO*VIN(IY)**2.)
  550 CONTINUE
        PAVG1(IY)=(P(5,IY)+P(6,IY)+P(7,IY)+P(8,IY))/4.
        PAVG2(IY)=(P(11,IY)+P(14,IY)+P(15,IY)+P(16,IY))/4.
        PAVG3(IY)=(P(17,IY)+P(18,IY)+P(19,IY)+P(20,IY))/4.
        PAVG4(IY)=(P(21,IY)+P(22,IY)+P(23,IY)+P(24,IY)+P(25,IY))/5.
        PAVG5(IY)=(P(26,IY)+P(27,IY)+P(28,IY))/3.
        PAVG6(IY)=(P(29,IY)+P(30,IY)+P(31,IY)+P(32,IY)+P(33,IY)+P(34,IY)+
```

```
1             P(35,IY))/7.
      PTOT(IY)=PT(IY)+(RHO*VFS(IY)**2.)/288.
      CPL(IY)=((PTOT(IY)-PAVG4(IY))*288.)/(RHO*VIN(IY)**2.)
      CPLF(IY)=((PTOT(IY)-PAVG4(IY))*288.)/(RHO*VFS(IY)**2.)
      CPLT(IY)=((PTOT(IY)-PAVG6(IY))*288.)/(RHO*VIN(IY)**2.)
      CPLTF(IY)=((PTOT(IY)-PAVG6(IY))*288.)/(RHO*VFS(IY)**2.)
      PLOC(IY)=PTOT(IY)-(RHO*VIN(IY)**2.)/288.
      SIGMA(IY)=((PLOC(IY)-PV)*288.)/(RHO*VIN(IY)**2.)
      RE(IY)=VIN(IY)*D/KV
400   CONTINUE
      WRITE (6,720) APnDEX
      WRITE (6,705)
      WRITE (6,700)  (RUN(IY),P(1,IY),P(2,IY),P(3,IY),P(4,IY),P(5,IY),
     1               P(6,IY),P(7,IY),P(8,IY),P(9,IY),IY=1,NRUNS)
      WRITE (6,706)
      WRITE (6,700)  (RUN(IY),P(10,IY),P(11,IY),P(12,IY),P(13,IY),
     1               P(14,IY),P(15,IY),P(16,IY),P(17,IY),P(18,IY),
     2               IY=1,NRUNS)
      WRITE (6,707)
      WRITE (6,700)  (RUN(IY),P(19,IY),P(20,IY),P(21,IY),P(22,IY),
     1   P(23,IY),P(24,IY),P(25,IY),P(26,IY),P(27,IY),IY=1,NRUNS)
      WRITE (6,708)
      WRITE (6,700)  (RUN(IY),P(28,IY),P(29,IY),P(30,IY),P(31,IY),
     1      P(32,IY),P(33,IY),P(34,IY),P(35,IY),Q(IY),IY=1,NRUNS)
      WRITE (6,710)
      WRITE (6,700)  (RUN(IY),PAVG1(IY),PAVG2(IY),PAVG3(IY),PAVG4(IY),
     1   PAVG5(IY),PAVG6(IY),CPF(1,IY),CPF(2,IY),CPF(3,IY),IY=1,NRUNS)
      WRITE (6,711)
      WRITE (6,700)  (RUN(IY),CPF(4,IY),CPF(9,IY),CPF(10,IY),CPF(11,IY),
     1CPF(12,IY),CPF(13,IY),CPI(17,IY),CPI(18,IY),CPI(19,IY),IY=1,NRUNS)
      WRITE (6,712)
      WRITE (6,700)  (RUN(IY),CPI(20,IY),CPI(21,IY),CPI(22,IY),
     1CPI(23,IY),CPI(24,IY),CPI(25,IY),CPI(26,IY),CPI(27,IY),CPI(28,IY),
     2   IY=1,NRUNS)
      WRITE (6,713)
      WRITE (6,700)  (RUN(IY),CPI(29,IY),CPI(30,IY),CPI(31,IY),CPI(32,IY)
     1      ,CPI(33,IY),CPI(34,IY),CPI(35,IY),VIN(IY),VFS(IY),IY=1,NRUNS)
      WRITE (6,714)
431   WRITE (6,700)  (RUN(IY),PTOT(IY),PLOC(IY),PT(IY),RE(IY),CPL(IY),
     1               CPLT(IY),SIGMA(IY),AREAA,D,IY=1,NRUNS)
      WRITE(6,725)
      WRITE(6,700)  (RUN(IY),PT(IY),VFS(IY),PTOT(IY),GPM(IY),VIN(IY),
     1 IVRA(IY),IVRB(IY),CPLF(IY),CPLTF(IY),IY = 1,NRUNS )
300   CONTINUE
700   FORMAT ((2X,I3,3X,9(E10.5E1,3X)))
701   FORMAT (I2)
702   FORMAT (I3)
704   FORMAT (6F10.4)
705   FORMAT (//*  RUN    P(1)          P(2)          P(3)          P(4)
     1      P(5)          P(6)          P(7)          P(8)          P(9)*/)
706   FORMAT (//*  RUN    P(10)         P(11)         P(12)         P(13)
     1      P(14)         P(15)         P(16)         P(17)         P(18)*/)
707   FORMAT (*1*//*  RUN    P(19)         P(20)         P(21)         P(22)
     1      P(23)         P(24)         P(25)         P(26)         P(27)
     2  */)
708   FORMAT (//*  RUN    P(28)         P(29)         P(30)         P(31)
     1      P(32)         P(33)         P(34)         P(35)         Q*/)
709   FORMAT ((2X,I3,3X,8(E10.5E1,3X)))
710   FORMAT (//*  RUN    PAVG1         PAVG2         PAVG3         PAVG4
     1      PAVG5         PAVG6         CPF(1)        CPF(2)        CPF(3)*/)
711   FORMAT (*1*//*  RUN   CPF(4)        CPF(9)        CPF(10)       CPF(1
     11)    CPF(12)       CPF(13)       CPI(17)       CPI(18)       CPI(19
     2)   */)
712   FORMAT (//*  RUN    CPI(20)       CPI(21)       CPI(22)       CPI(23)
     1      CPI(24)       CPI(25)       CPI(26)       CPI(27)       CPI(28)
     2 */)
```

```
713 FORMAT (*1*//*  RUN   CPI(29)      CPI(30)      CPI(31)      CPI(3
   12)      CPI(33)      CPI(34)      CPI(35)      V(INLET)     VFS*/)
714 FORMAT (//*  RUN  P(TOTAL)     P(LOCAL)     P(TUNNEL)     REYNOLDS
   1NO. CPL(LOWER)   CPL(TOP)     SIGMA(IN)    AREAA         D */)
715 FORMAT (I5)
716 FORMAT (2F10.5)
717 FORMAT (*1*//41H   THE FOLLOWING DATA REFERS TO DATA SET ,I2/)
718 FORMAT (I3,7X,5F10.3)
719 FORMAT (3A10)
720 FORMAT (/20H      POD POSITION = ,A10)
721 FORMAT (F10.4)
722 FORMAT (I3,7X,4E11.5E1)
723 FORMAT (I3,7X,5E11.5E1)
725 FORMAT (*1*//*  RUN   P(TUNNEL)    V(TUNNEL)    P(TOTAL)     FLOW(
   1GPM)    V(INLET)      IVR(ACTUAL)  IVR(CRUISE)  P-LOSS(LOW)  P-LOSS
   2(TOP)*/)
727 FORMAT (I3,7X,6E11.5E1)
732 FORMAT (I3,7X,2E11.5E1)
735 FORMAT (E10.5)
    STOP
    END
0000000000000000000000
```

APPENDIX E

LISTING OF DATA REDUCTION PROGRAM USED FOR ANALYSIS OF FORCE DATA

```
      PROGRAM  WJETD(INPUT,OUTPUT,TAPE5=INPUT,TAPE6=OUTPUT)
C AL SOBOLEWSKI     CODE 1532    X71318
C  DSI WATERJET INLET DATA REDUCTION PROGRAM
      DIMENSION          GPM(25),DRAG(25),VT(25),PT(25),SIGMA(25),
     2  AIVR(25),BIVR(25),VIA(25),VIB(25),XDRAG(25),CD(25),XLIFT(25),
     3  PTF(25),PI(25),PE(25),VE(25),Q(25),CL(25),FE(25),FI(25),
     4  CDMO(25),CDME(25),CLMO(25),CLME(25),CFE(25),CFI(25)
      REAL LIFT(25),MOMI(25),MOML(25)
      INTEGER PODEX,ASIGMA,APODEX,AFSS,RUN(25)
      READ (5,508) RHO,CF,PV,H
      READ (5,509) AREAE,AREAS,AREAB
      READ(5,516) NGRAPHS
      DO 36 J=1,NGRAPHS
      WRITE(6,549) J
C
      READ(5,570) ASIGMA,APODEX,AFSS
C
      READ (5,511) PODEX
      IF (PODEX-412) 931,932,933
  931 AREAA=0.03097
      GO TO 935
  932 AREAA=0.03431
      GO TO 935
  933 IF (PODEX-1057) 936,937,938
  936 AREAA=0.05139
      GO TO 935
  937 AREAA=0.06781
      GO TO 935
  938 AREAA=0.08177
  935 CONTINUE
      READ (5,512) NPTS
      READ (5,513) (RUN(IA),GPM(IA),DRAG(IA),LIFT(IA),VT(IA),PT(I
     1              IA=1,NPTS)
      DO 300 IX=1,NPTS
C  COMPUTE INLET VELOCITY AND IVR FOR ACTUAL AND CRUISE AREA
      Q(IX)=GPM(IX)*CF
      VIA(IX)=Q(IX)/AREAA
      VIB(IX)=Q(IX)/AREAB
      BIVR(IX)=VIB(IX)/VT(IX)
      AIVR(IX)=VIA(IX)/VT(IX)
C  COMPUTE EXTERNAL DRAG AND DRAG COEFFICIENT
      DEN=.5*RHO*AREAS*VT(IX)**2.
      MOMI(IX)=RHO*Q(IX)*VIA(IX)
      XDRAG(IX)=DRAG(IX)-MOMI(IX)
      CD(IX)=XDRAG(IX)/DEN
      CDMO(IX)=MOMI(IX)/DEN
      CDME(IX)=DRAG(IX)/DEN
C  COMPUTE SIGMA
      PT(IX)=PT(IX)*144.
      SIGMA(IX)=(PT(IX)-PV)/(.5*RHO*VT(IX)**2.)
C  COMPUTE EXTERNAL LIFT AND LIFT COEFFICIENT
      VE(IX)=Q(IX)/AREAE
      MOML(IX)=RHO*Q(IX)*VE(IX)
      XLIFT(IX)=LIFT(IX)-MOML(IX)
      CL(IX)=XLIFT(IX)/DEN
      CLMO(IX)=MOML(IX)/DEN
      CLME(IX)=LIFT(IX)/DEN
C  COMPUTE PRESSURES P(INLET) AND P(EXIT)
      PTF(IX)=PT(IX)+.5*RHO*VT(IX)**2.
      PI(IX)=PTF(IX)-.5*RHO*VIA(IX)**2.
      PE(IX)=PTF(IX)-.5*RHO*VE(IX)**2.+RHO*32.2*H
C  COMPUTE PRESSURE FORCE AT INLET AND EXIT
      FE(IX)=(PE(IX)-PT(IX))*AREAE
      FI(IX)=(PI(IX)-PT(IX))*AREAA
```

```
      CFE(IX)=FE(IX)/DEN
      CFI(IX)=FI(IX)/DEN
  300 CONTINUE
      WRITE(6,592)
      WRITE(6,594) ASIGMA,APODEX,AFSS
      WRITE(6,595) NPTS
      WRITE(6,590)
      WRITE(6,591) (RUN(IX),VIA(IX),VIB(IX),AIVR(IX),BIVR(IX),MOMI(IX),
     1             XDRAG(IX),CD(IX),CDMO(IX),CDME(IX),PT(IX),SIGMA(IX),
     2             VE(IX),IX=1,NPTS)
      WRITE(6,596)
      WRITE(6,597) (MOML(IX),XLIFT(IX),CL(IX),CLMO(IX),CLME(IX),PTF(IX),
     1             PI(IX),PE(IX),FE(IX),FI(IX),CFE(IX),CFI(IX),
     2             IX=1,NPTS)
C
   36 CONTINUE
  508 FORMAT (4F10.4)
  509 FORMAT (3F10.5)
  511 FORMAT (I5)
  512 FORMAT (I3)
  513 FORMAT (I3,7X,5F10.3)
  516 FORMAT(I2)
  549 FORMAT(//////41H FOLLOWING DATA PERTAINS TO GRAPH NUMBER ,I2)
  570 FORMAT(3A10)
  590 FORMAT (///* RUN NO.   VIA        VIB        AIVR       BIVR       MOM
     1I       DRAG(EX)   CD(EX)     CDMO       CDME       PT         SIGMA
     2 VE*/)
  591 FORMAT ((1X,I7,3X,2(F7.2,3X),2(F7.5,3X),2(F7.2,3X),3(F7.5,3X),
     1        F7.2,3X,2(F7.3,3X)))
  592 FORMAT (//*      DSI WATERJET DRAG DATA *)
  594 FORMAT (/30H              TEST COND. - SIGMA = ,A10,15HPOD POSITION = ,
     1         A10,20H FULL SCALE SPEED = ,A10)
  595 FORMAT (/20H             NO. PTS. = ,I3)
  596 FORMAT (///* LIFT(MOM) LIFT(EX)  CL(EX)     CLMO       CLME       PTF
     1      PI         PE         FE         FI         CFE        CFI*/)
  597 FORMAT ((1X,2(F7.2,3X),3(F7.5,3X),5(F7.2,3X),2(F7.5,3X)))
      STOP
      END
0000000000000000000000
```


©U.S. GOVERNMENT PRINTING OFFICE: 1977 240-824/008 1-3

END

AD-A038 590 DAVID W TAYLOR NAVAL SHIP RESEARCH AND DEVELOPMENT CE--ETC F/G 13/7
HYDRODYNAMIC PERFORMANCE OF THE MODEL OF A VARIABLE AREA WATERJ--ETC(U)
FEB 77 A D SOBOLEWSKI

UNCLASSIFIED SPD-735-01 NL

2 OF 2

AD A038 590

SUPPLEMENTARY INFORMATION

END

DATE FILMED

10-77

DDC

2 OF 2

AD
A038 590

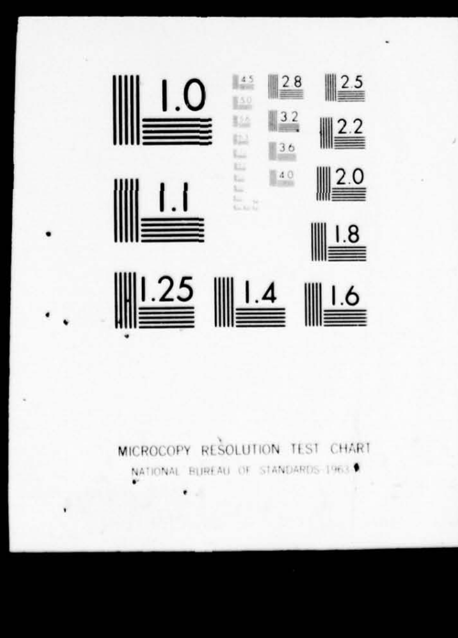

SUPPLEMENTARY

INFORMATION

AD-A038 590

DEPARTMENT OF THE NAVY
NAVAL SHIP RESEARCH AND DEVELOPMENT CENTER
HEADQUARTERS
BETHESDA, MARYLAND 20084

ANNAPOLIS LABORATORY
ANNAPOLIS, MD 21402
CARDEROCK LABORATORY
BETHESDA, MD 20084

IN REPLY REFER TO:

1532:MLR
28 Apr 1977

From: Commander, David W. Taylor Naval Ship R&D Center
To: Distribution List

Subj: Ship Performance Department Report, SPD-735-01

Encl: (1) Errata Sheet for Ship Performance Dept. Report SPD-735-01, "Hydrodynamic Performance of the Model of a Variable Area Waterjet Inlet Designed for a 200 Ton, 100 Knot Hydrofoil Ship, by Alan D. Sobolewski, Feb 1977

1. Please replace the Administrative Information in the above report with the enclosed sheet.

Gabor F. Dobay
Gabor F. Dobay

Copy to:

NAVMAT
Code 0333 (Vittucci)

NAVSEC
Code 6110 (Leopold)
6114 (Johnson)
6114P (Kerr)
6136 (Keane)
(Conrad)
6141B (Graves)
6144 (Welling)
6144E (Lombardi)

NAVSEA
Code 0322 (Schuler)
(Senen)
(Dilts)
0331 (Chaikin)
(Miller)

NAVSEA
Code 035 (Sorkin)
0351 (Peirce)
PMS 304.20 (Schuldenfrei)
PMS 304.31E

DDC

ADMINISTRATIVE INFORMATION

The project was sponsored by the Naval Sea Systems Command under the following Codes, Task Areas, and Program Elements:

FY	Code	Task Area	Task	Element
75	0331G	SF43270208	17867	62543N
75	03411	S324613	17713	63508N
76	0331G	SF43432301	12501	62543N